Cell

Telomeric 3′ Overhangs Derive from Resection by Exo1 and Apollo and Fill-In by POT1b-Associated CST

Peng Wu,[1] Hiroyuki Takai,[1] and Titia de Lange[1,*]
[1]Laboratory for Cell Biology and Genetics, The Rockefeller University, 1230 York Avenue, New York, NY 10065, USA
*Correspondence: delange@mail.rockefeller.edu
http://dx.doi.org/10.1016/j.cell.2012.05.026

SUMMARY

A 3′ overhang is critical for the protection and maintenance of mammalian telomeres, but its synthesis must be regulated to avoid excessive resection of the 5′ end, which could cause telomere shortening. How this balance is achieved in mammals has not been resolved. Here, we determine the mechanism for 3′ overhang synthesis in mouse cells by evaluating changes in telomeric overhangs throughout the cell cycle and at leading- and lagging-end telomeres. Apollo, a nuclease bound to the shelterin subunit TRF2, initiates formation of the 3′ overhang at leading-, but not lagging-end telomeres. Hyperresection by Apollo is blocked at both ends by the shelterin protein POT1b. Exo1 extensively resects both telomere ends, generating transient long 3′ overhangs in S/G2. CST/AAF, a DNA polα.primase accessory factor, binds POT1b and shortens the extended overhangs produced by Exo1, likely through fill-in synthesis. 3′ overhang formation is thus a multistep, shelterin-controlled process, ensuring functional telomeric overhangs at chromosome ends.

INTRODUCTION

A conserved feature of telomeres is a 3′ overhang composed of G-rich repeats that protrude beyond the complementary C-rich telomeric repeat strand. TTAGGG repeat overhangs of 30–400 nt are present at both ends of each mammalian chromosome (Makarov et al., 1997; McElligott and Wellinger, 1997; Chai et al., 2006) and contribute to telomere function by binding the POT1 components of the telomeric shelterin complex, serving as primers for telomerase, and forming the t-loop structure (Palm and de Lange, 2008). At the telomeres generated by lagging-strand DNA synthesis (lagging-end telomeres), overhangs of up to 200 nt could potentially originate from an inability of the DNA polα.primase complex to initiate Okazaki fragment synthesis efficiently at the end of a linear DNA template, a deficiency that has been observed in vitro (Ohki and Ishikawa, 2004). However, leading-strand DNA synthesis is expected to generate a blunt end that requires additional processing to mature into a functional telomere terminus.

The significance of overhang generation is not only in the maintenance of a protected telomere state but also relates to cellular aging. The 5′ end resection needed to generate a 3′ overhang at leading-end telomeres could contribute significantly to telomere shortening, compounding the ''end-replication problem,'' which refers to incomplete replication by lagging-strand synthesis. In agreement, the rate of telomere shortening in telomerase-deficient human cells correlates with the average length of the telomeric overhang (Huffman et al., 2000). Because telomere attrition rates determine the replicative lifespan of telomerase-deficient human cells, the postreplicative processing of telomere ends could affect cellular aging and thus govern the telomere tumor suppressor pathway (Artandi and DePinho, 2010).

Despite a wealth of information on telomere end processing in yeast (Longhese et al., 2010), relatively little is known about how the mammalian telomeric overhangs are generated. In telomerase-negative human cells, overhangs at leading-end telomeres appear to be shorter than those at lagging-end telomeres, whereas the presence of telomerase equalizes this size distribution (Makarov et al., 1997; McElligott and Wellinger, 1997; Chai et al., 2006). The terminal nucleotides on the C-rich strand are remarkably precise, ending in 3′-CCAATC-5′ at >80% of leading- and lagging-end telomeres (Sfeir et al., 2005). This suggests that 5′ end processing of leading- and lagging-end telomeres is highly regulated and includes a common final step (Sfeir et al., 2005). In contrast, the last nucleotides of the G-rich strand are variable, although TAG-3′ ends predominate when telomerase is active (Sfeir et al., 2005). Although telomeric overhangs can be detected in all stages of the cell cycle, the telomeric overhang signal increases in late S/G2 phase, presumably due to resection of the C-rich strand (Dai et al., 2010).

The Apollo/SNM1B nuclease has been proposed to affect telomere end processing, specifically at leading-end telomeres (Wu et al., 2010; Lam et al., 2010). Apollo is recruited to telomeres by the shelterin subunit TRF2 (Chen et al., 2008; van Overbeek and de Lange, 2006; Lenain et al., 2006; Bae et al., 2008). Absence of Apollo results in a 25%–35% reduction in the overhang signal, which was proposed to be due to diminished processing of the leading-end telomeres because of the

propensity of Apollo-depleted leading-end telomeres to fuse (Wu et al., 2010; Lam et al., 2010).

A second factor regulating the overhang is POT1, the single-stranded (ss) DNA binding factor in shelterin. Knockdown of human POT1 abolishes the specification of the telomeric 5′ end and reduces the telomeric overhang signal by 20%–30% (Hockemeyer et al., 2005). However, the interpretation of this data is confounded by the concomitant activation of the DNA damage response, which could induce aberrant processing at the POT1-depleted telomeres. Less ambiguous information emerged from the analysis of mouse shelterin, which unlike human telomeres has two POT1 proteins (POT1a and POT1b) that evolved distinct functions, such that POT1b regulates the telomeric overhang, whereas POT1a represses ATR signaling (Hockemeyer et al., 2006; Denchi and de Lange, 2007; Guo et al., 2007; Wu et al., 2006). POT1b deletion results in long ss telomeric overhangs and accelerated telomere shortening but no DNA damage signal (Hockemeyer et al., 2006, 2008; He et al., 2009). POT1b was proposed to limit degradation of the telomeric C-rich strand, but the nuclease(s) responsible for aberrant processing have not been identified.

A third factor involved in modulating the telomeric overhang is the CST/AAF complex, composed of the oligosaccharide/oligonucleotide binding (OB)-fold-containing proteins Ctc1, Stn1 (also referred to as OBFC1), and Ten1 (Surovtseva et al., 2009; Miyake et al., 2009; Goulian et al., 1990). Based on structural similarities, CST/AAF is proposed to be the ortholog of the budding yeast telomeric CST complex (also known as t-RPA), an RPA-like complex composed of Cdc13, Stn1, and Ten1 (Gao et al., 2007). Human Ctc1 and Stn1 were originally identified as the AAF132 and AAF44 accessory factors of DNA polα.primase, which stimulate de novo RNA primer synthesis as well as primer-dependent elongation in reconstituted DNA replication systems (Goulian et al., 1990; Casteel et al., 2009). Human CST/AAF can localize to telomeres, potentially through an interaction with the shelterin protein TPP1 (Wan et al., 2009), and its depletion increases the ss telomeric DNA (Dai et al., 2010; Miyake et al., 2009; Surovtseva et al., 2009).

Here, we document the combinatorial action of Apollo, POT1b, CST, and the 5′ exonuclease Exo1 in postreplicative telomere end processing in mouse cells, clarifying the mechanism by which the mammalian telomeric 3′ overhang is generated and modulated.

RESULTS

Apollo Specifically Affects the Overhangs of Leading-End Telomeres

To further define the role of Apollo in telomere end processing, we adapted the use of CsCl density gradient equilibrium centrifugation to separate the telomeres synthesized by leading- and lagging-strand DNA synthesis based on their different incorporation of BrdU (Figures 1A and 1B) (Chai et al., 2006). Fractionated DNA from BrdU-labeled mouse embryonic fibroblasts (MEFs) revealed distinct peaks of telomeric signal intensity corresponding to the unreplicated, lagging-end, leading-end, and (rarely) doubly replicated telomeres (Figure 1B). The densities of unreplicated and doubly substituted telomeric DNA were confirmed with DNA isolated from untreated cells or cells incubated with BrdU for 48 hr (Figures S1A and S1B available online).

Pooled fractions representing leading- and lagging-end telomeres were analyzed by in gel native DNA hybridization with an oligonucleotide complementary to TTAGGG repeats to detect the 3′ overhangs (Figure 1C). After capture of the signal, the DNA was denatured in situ and rehybridized with the same probe in order to determine the total telomeric signal for normalization of the ss TTAGGG signal in each lane. Although this method does not directly evaluate the length of the telomeric overhangs, it is generally assumed that changes in the normalized overhang signals reflect changes in overhang lengths.

As the separated leading- and lagging-end telomere fractions represent fully replicated TTAGGG repeat arrays, they are not expected to contain replication intermediates. Therefore, the ss TTAGGG signal should be primarily derived from the 3′ overhang. Indeed, in the fractions containing leading- and lagging-end telomeres, there is very little ss telomeric signal outside of the bracketed (quantified) regions, whereas the bulk telomeres show additional signal smearing upward that may represent replication intermediates (Figure 1C).

Detection of the telomeric overhang signal revealed that in Apollo-deficient cells, the overhangs at leading-end telomeres were reduced by ~50%, whereas lagging-end overhangs were unaffected (Figures 1C and 1D). The severity of the overhang defect at leading-end telomeres in the absence of any defect in lagging-end overhangs is consistent with the 20%–35% reduction in overhang signal detected in bulk DNA isolated from Apollo-deficient cells (Wu et al., 2010; Lam et al., 2010). Thus, Apollo contributes to overhang generation specifically at leading-end telomeres.

In cells with normal Apollo levels, the ratio of the overhangs at leading- and lagging-end telomeres was affected by the telomerase status. When telomerase was absent ($mTR^{-/-}$ cells), leading- and lagging-end telomeres show equal overhangs, whereas in cells with telomerase activity ($mTR^{+/+}$ cells), the overhangs at leading-end telomeres were 30%–50% longer than the overhangs at the lagging-end telomeres (Figure 1D and Figure S1C). The studies below on the impact of Exo1, CST, and POT1b on the bulk overhang signals were performed in both telomerase-proficient and -deficient cells with essentially the same results. The effect of Apollo on the telomeric overhang was previously shown to be independent of telomerase (Wu et al., 2010).

Exo1 Mediates Formation of Transiently Extended Overhangs after DNA Replication

It was previously shown that the overhang signal in mouse and human cells transiently increases ~2-fold in S/G2 (Dai et al., 2010; Wu et al., 2010) (Figure 2C below). Using a previously developed FUCCI-based system to isolate cells in G1 and S/G2 (Wu et al., 2010), we verified that the 3′ overhang signal was 1.5- to 2-fold greater in S/G2 than in G1 and found this to be the case regardless of telomerase status (Figures 2A–2C). The signals were sensitive to digestion with *Escherichia coli* 3′ exonuclease, confirming that they represented the 3′ overhang rather than internal ss DNA formed during replication (Figure 2A).

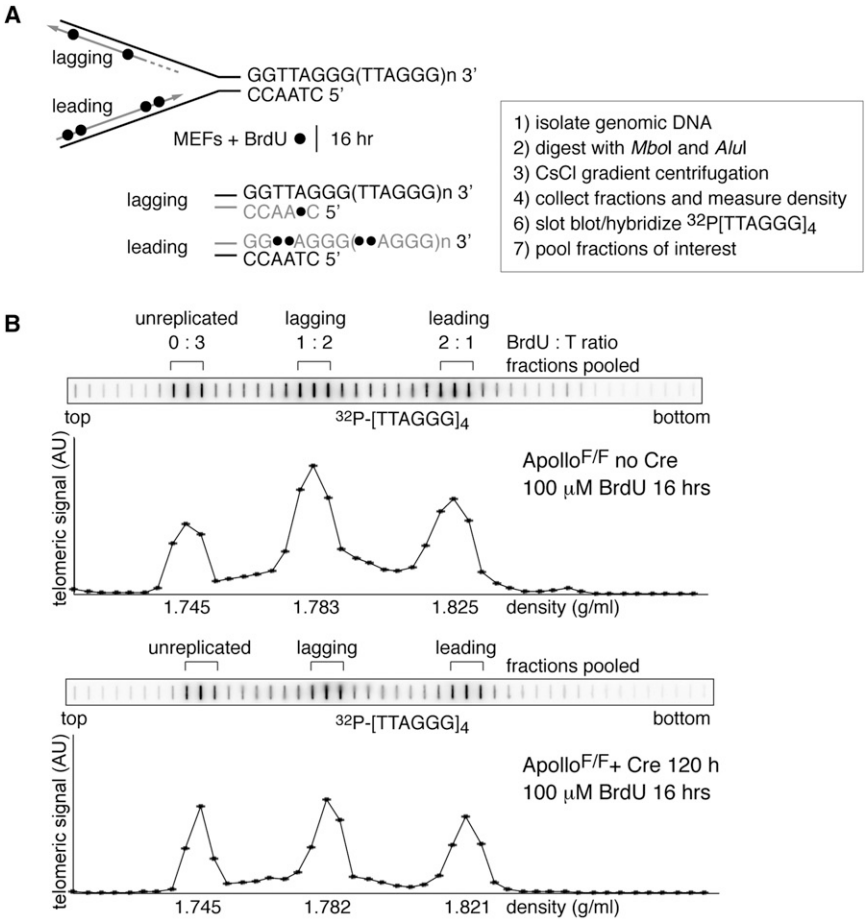

Figure 1. Apollo Contributes to Overhang Generation at Leading-End Telomeres

(A and B) Separation of leading- and lagging-end telomeres. DNA from BrdU labeled MEFs (e.g., Apollo$^{F/F}$ at 120 hr after Cre or without Cre) was digested and fractionated by CsCl density gradient equilibrium centrifugation.

(B) Telomeric signals in slot-blotted gradient fractions (plotted in arbitrary units) and CsCl densities calculated from the refractive index. Fractions pooled for overhang analyses are indicated.

(C) Overhang analysis of separated leading- and lagging-end telomeres fractionated by pulse-field gel electrophoresis. ss telomeric signal was detected by annealing a ^{32}P-[AACCCT]$_4$ probe to native DNA. After capture of the signal, the DNA was denatured in situ and rehybridized with the same probe to capture the total telomeric DNA signal for normalization of each lane. The bracketed region was used for quantification of all the gels; the trends were the same when the entire lanes were used for quantification. Asterisks indicate presumed interstitial telomeric fragments that differentially fractionate with the leading- or lagging-end telomeres providing an internal control for the gradients. Numbers under the lanes indicate the relative normalized overhang signals with the underlined lane set to 1.

(D) Quantification of the telomeric overhang signal as detected in (C). Mean and SDs of three or more independent experiments. ** indicates $p < 0.05$ (paired student's t test). Bar labeled ref is the reference value (set to 1). See also Figure S1.

Exonuclease 1 has been implicated as one of the nucleases mediating 5′ end resection at DNA double-strand breaks (DSBs) (Mimitou and Symington, 2008; Zhu et al., 2008; Gravel et al., 2008) and in the generation of ss DNA at chromosome ends in late-generation telomerase knockout mice (Schaetzlein et al., 2007). Although we and others previously reported that Exo1 has no effect on the telomeric overhang signal in mouse fibroblasts (Hockemeyer et al., 2008; Schaetzlein et al., 2007), we found that absence of Exo1 from asynchronous mTR$^{-/-}$ and mTR$^{+/+}$ MEFs resulted in a 30%–40% reduction in the overhang signal (Figures 2A–2C). Furthermore, Exo1 deficiency significantly altered the cell-cycle-dependent changes in overhang signal, resulting in a minimal increase in the overhang signal in S/G2 (Figures 2A–2C). The transient elongation of the overhangs in S/G2 depends on Exo1 in both telomerase-proficient and -deficient cells (Figures 2B and 2C). Thus, Exo1 is largely responsible for the telomerase-independent increase in ss telomeric DNA that occurs after DNA replication. The residual transient increase in the overhang signal that occurs in S/G2 in Exo1$^{-/-}$mTR$^{-/-}$ cells may reflect the processing of leading-end telomeres by Apollo and/or the formation of an extended overhang at lagging-end telomeres as a consequence of incomplete replication. Prior studies suggesting that Exo1 status does not affect the overhang signal may have used cell populations with a low S phase index.

Unlike Apollo, Exo1 appeared to exert its effect on both leading- and lagging-end telomeres. Exo1 deficiency resulted in a 40% reduction in the telomeric overhang signal at both newly

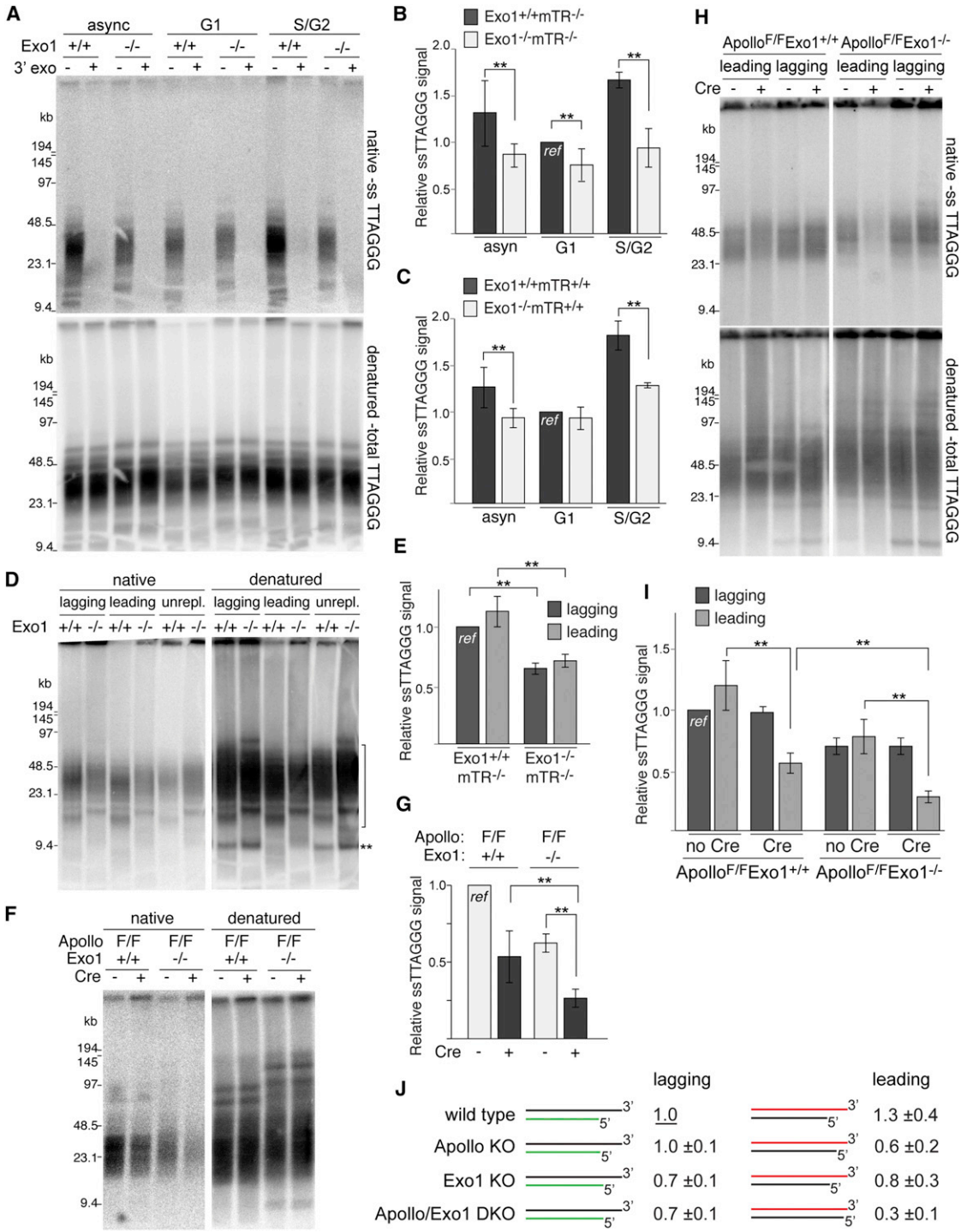

Figure 2. Exo1 Contributes to Transient Overhang Elongation in Late S Phase

(A and B) Overhang assay on Exo1$^{+/+}$mTR$^{-/-}$ and Exo1$^{-/-}$mTR$^{-/-}$ MEFs in G1 and S/G2 isolated by FUCCI-FACS. See legend of Figure 1 for details.

(C) Quantification of relative overhang signals in Exo1$^{+/+}$mTR$^{+/+}$ and Exo1$^{-/-}$mTR$^{+/+}$ MEFs in G1 and S/G2 (as in A and B).

(D and E) Overhang analysis of leading-, lagging-end and unreplicated telomeres from Exo1$^{+/+}$mTR$^{-/-}$ and Exo1$^{-/-}$mTR$^{-/-}$ MEFs.

(F and G) Overhang analysis of Apollo$^{F/F}$Exo1$^{+/+}$ and Apollo$^{F/F}$Exo1$^{-/-}$ MEFs at 120 hr after Hit&Run Cre.

(H and I) Overhang analysis of leading- and lagging-end telomeres from Apollo$^{F/F}$ and Apollo$^{F/F}$Exo1$^{-/-}$ MEFs without Cre or at 120 hr after Hit&Run Cre. Slot blots of the gradients are shown in Figure S2.

(J) Relative overhang size in WT, Apollo KO, Exo1 KO, and Apollo/Exo1 DKO MEFs.

All quantifications show means and SDs of three or more independent experiments. ** indicates $p < 0.05$ (paired student's t test). See also Figures S2 and S3.

synthesized telomeres (Figures 2D and 2E). In contrast, the overhang signal at the unreplicated telomeres, representing the overhang status in G1, showed no decrease in Exo1-deficient cells.

We derived Apollo$^{F/F}$Exo1$^{-/-}$ conditional double-knockout (DKO) cells to determine the effect of the combined absence of Apollo and Exo1. Whereas absence of either Apollo or Exo1 alone resulted in a 30%–50% reduction in the overhang signal, cells lacking both nucleases had an overhang signal that was reduced by 70% compared to wild-type cells (Figures 2F and 2G). Codeletion of Apollo and Exo1 had an additive effect on the overhang signal at leading- but not lagging-end telomeres, as expected from the leading-end specificity of Apollo (Figures 2H–2J; Figures S2A–S2D).

We also explored the role in telomere end processing of NBS1 and BLM, whose orthologs contribute to DSB processing in budding yeast (Gravel et al., 2008; Mimitou and Symington, 2008; Zhu et al., 2008). However, deletion of either NBS1 or BLM from MEFs did not reduce the overhang signal significantly even when Exo1 was absent (Figures S2E–S2H).

Interestingly, Exo1-deficient cells showed no signs of telomere dysfunction as reflected by the phosphorylation of Chk2, formation of telomere dysfunction-induced foci (TIFs), or telomere fusions (Figures S3A–S3D). This is in contrast to the phenotype associated with loss of Apollo, which results in the appearance of ATM-dependent TIFs at a subset of telomeres in S phase and gives rise to fusions between leading-end telomeres (Wu et al., 2010; Lam et al., 2010) (Figures S3C–S3E). These results would be consistent with Exo1 acting at a step subsequent to the initial processing steps required to maintain end protection or could be explained by Exo1 being redundant with other processing factors.

In addition, Exo1 deficiency did not exacerbate the telomere dysfunction phenotypes associated with Apollo deletion (Figures S3C–S3E). Taken together, these results suggest that Exo1 does not require Apollo to act at telomeres. However, the apparent Apollo-independent action of Exo1 may in part be due to the DNA damage response (DDR) at leading-end telomeres in cells lacking Apollo. In the absence of Apollo, the DDR at leading-end telomeres could mediate the initial resection needed for Exo1 to act (Mimitou and Symington, 2008; Zhu et al., 2008) and/or facilitate Exo1 recruitment.

The data above suggested that after Exo1 generates extended overhangs in S/G2, additional events decrease the overhang length resulting in the lowered overhang signal in G1. Consistent with this interpretation of the data, there was no attenuation of the telomere shortening rate in cells deficient in both Exo1 and mTR compared to cells lacking telomerase only (Figures S3F and S3G). Thus, the amount of sequence lost with every cell division does not primarily depend on Exo1-mediated processing, implying subsequent step(s) in telomere processing that removes the long overhangs and shortens them to their G1 size.

CST Contributes to the Postreplicative Correction of the Overhang

Because the shortening of the overhangs could be due to fill-in synthesis, we examined the role of CST/AAF, which has been implicated in both overhang regulation and DNA polα.primase function (Dai et al., 2010; Miyake et al., 2009; Surovtseva et al., 2009; Goulian et al., 1990; Casteel et al., 2009). To inhibit Stn1, we used an shRNA that resulted in an obvious reduction in Stn1 levels based on immunoblotting with a mouse polyclonal antibody raised against full-length recombinant mouse Stn1 (Figure 3A) but did not affect the cell-cycle profile or proliferation at the early time points used for this analysis. Importantly, the shRNA treated cells did not display TIFs (<3% cells with >5 TIFs; $n > 50$) or chromosome end fusions (<1% of chromosomes; $n > 1{,}000$), indicating that their telomere function was not overtly compromised. However, Stn1 depletion in both telomerase-deficient and -proficient cells showed a nearly 2-fold increase in the relative ss telomeric DNA detected by in gel hybridization (Figures 3B and 3C and Figure S4A; see Figures 3F and 3G below). The signal could be attributed to the 3′ overhang because it was removed by *E. coli* 3′ exonuclease. Furthermore, repression of Ctc1 with an shRNA increased the overhang signal (Figure S4A).

To address whether Stn1 was involved in the correction of the overhangs created in late S/G2, telomerase-deficient cells depleted of Stn1 were sorted by using the FUCCI system (Figures 3B and 3C). The results indicated that Stn1-depleted cells had aberrantly high overhang signals in G1 (Figure 3C). Meanwhile, Stn1 depletion resulted in only a modest increase in the overhang signal in S/G2 compared to control cells in that phase ($p > 0.05$). Furthermore, Stn1-depleted cells did not show a significant difference in overhang signals in G1 and S/G2 ($p > 0.05$) (Figure 3C). Thus, the depletion of Stn1 leads to aberrant overhangs primarily in G1, which is consistent with Stn1 contributing to the restoration of the transiently elongated overhangs formed in S/G2.

Stn1 depletion did not overtly compromise the semiconservative replication of bulk telomeres because there were no changes in the CsCl profiles (Figure S4B). However, depleting Stn1 resulted in a 1.6-fold increase in the lagging-end overhangs and a 1.2-fold increase in the leading-end overhangs (Figures 3D and 3E). Thus, the data suggest that Stn1 acts at both newly synthesized telomeres to correct the excessive overhangs generated in late S phase. Although the shRNA experiments are unlikely to reveal the full extent of the null phenotype of Stn1, the same conclusion was reached based on experiments in which Stn1 was blocked from associating with telomeres (see below).

Because these results suggested that Apollo and Exo1 contribute to the generation and lengthening of overhangs in S phase, whereas CST restores the long overhangs to their G1 size, we investigated the effect of depleting Stn1 in cells lacking both Apollo and Exo1. When Stn1 was depleted from cells lacking Apollo, a 1.7-fold increase in the overhang signal was observed, similar to what occurs in wild-type cells depleted of Stn1 (Figures 3F and 3G). However, in cells lacking Exo1, the increase in overhang signal upon Stn1 depletion was only 1.3-fold, a result that was independent of the status of Apollo (Figures 3F and 3G). These data suggest that a major role for CST is to correct the excessive overhangs generated by Exo1. However, even in the absence of Exo1 and Apollo, CST

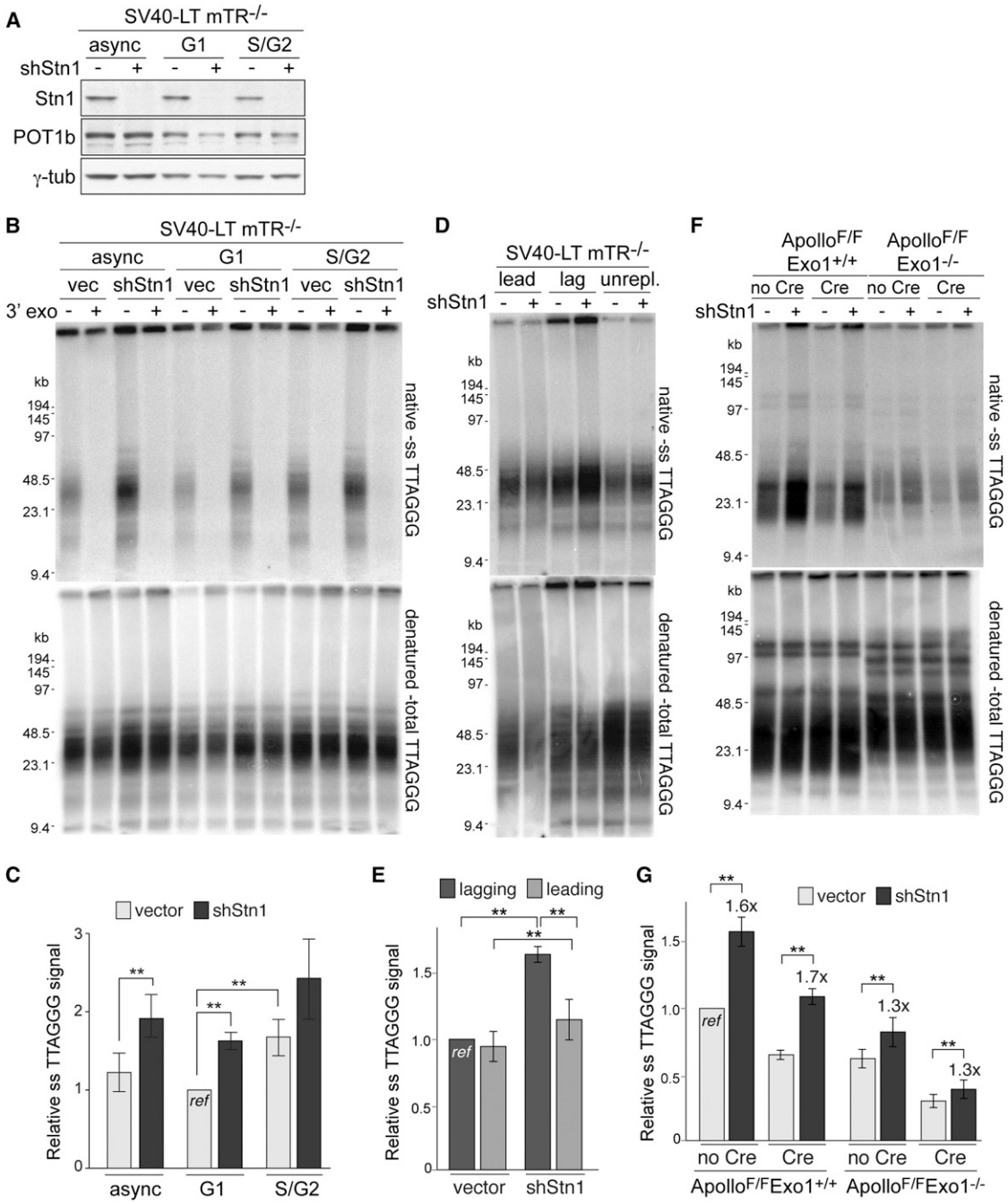

Figure 3. Stn1 Restores Overhangs to Their G1 Size

(A) Immunoblot for Stn1 and POT1b in asynchronous mTR$^{-/-}$ MEFs or in cells in G1 and S/G2 isolated by FUCCI-FACS at 96 hr after Stn1 shRNA.

(B and C) Overhang analysis of the cells described in (A). See legend of Figure 1 for details.

(D and E) Overhang analysis of leading- and lagging-end telomeres from mTR$^{-/-}$ MEFs at 96 hr after Stn1 shRNA. See Figure S4B CsCl gradient slot blots.

(F and G) Overhang assay of Apollo$^{F/F}$ and Apollo$^{F/F}$Exo1$^{-/-}$ MEFs at 96 hr after Stn1 shRNA to Stn1 and at 120 hr after Hit&Run Cre.

All quantifications show means and SDs of three or more independent experiments. ** indicates $p < 0.05$ (paired student's t test). See also Figure S4.

contributes to limiting overhang length, possibly by fill-in synthesis that restores excessive overhangs generated by other, still unidentified nucleases and/or incomplete lagging-strand DNA synthesis.

POT1b Controls the Overhang at Both Newly Synthesized Telomeres

Prior work has shown that POT1b deletion increases the overhang signal in a manner that is independent of telomerase

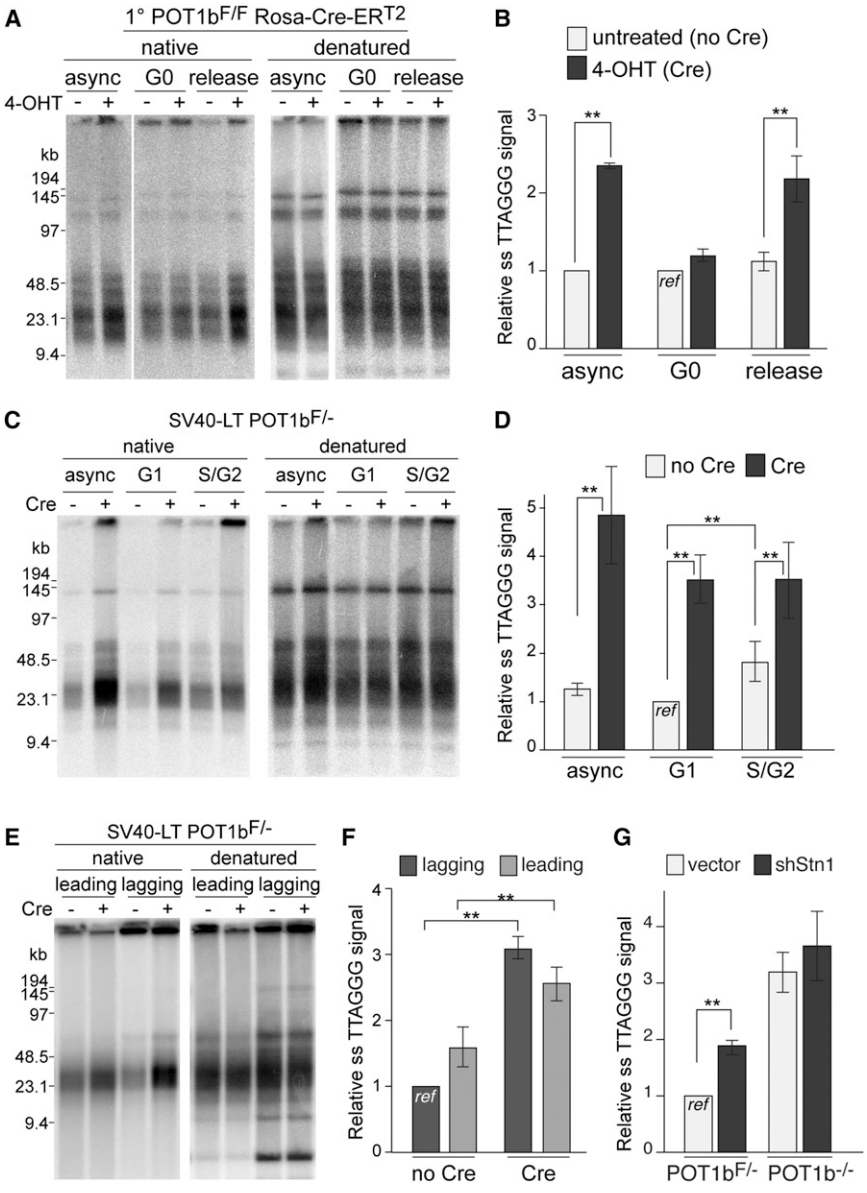

Figure 4. POT1b Regulates Overhangs at Both Sister Telomeres

(A and B) Overhang assay of asynchronous, G0 arrested, and released 1° POT1b$^{F/F}$ ROSA26-Cre-ER^{T2} MEFs with and without Cre induction (4-OHT). Values represent the mean of two experiments using independent POT1b$^{F/F}$ ROSA-Cre-ER^{T2} MEF lines and SEM. See legend of Figure 1 for details.

(C and D) Overhang analysis of POT1b$^{F/-}$ cells at 120 hr post Cre in G1 and S/G2 isolated by FUCCI-FACS.

(E and F) Overhang analysis of leading- and lagging-end telomeres from POT1b$^{F/-}$ MEFs at 120 hr post-Cre (or withouit Cre). For slot blots of the CsCl gradient, see Figure S4C.

(G) Quantification of overhang analyses of POT1b$^{F/-}$ MEFs at 96 hr following lentiviral shRNA to Stn1 and 120 hr after Hit&Run Cre treatment. The signal in POT1b$^{F/-}$ MEFs without Cre is set to 1. Mean of three independent experiments and SDs. See also Figure S4.

(Hockemeyer et al., 2008). We determined whether POT1b functions, like Apollo, Exo1, and CST in the regulation of postreplicative telomere end processing. Consistent with such a role, removal of POT1b resulted in an increase in the telomeric overhang signal in cycling cells but not in contact-inhibited, serum-starved primary MEFs kept in G0 (Figures 4A and 4B). Importantly, no difference was observed in the overhang signal in POT1b-deficient cells in G1 or S/G2 (Figures 4C and 4D). Separation of leading- and lagging-end telomeres showed that POT1b deletion induced a ~2-fold increase in the overhang signal at leading-end telomeres and a ~3-fold increase in the overhang at lagging-end telomeres (Figures 4E and 4F and Figure S4C), indicating that POT1b plays a role at both newly synthesized telomeres.

The defect in the postreplicative restoration of overhangs in POT1b-deficient cells is reminiscent of the effect of Stn1 depletion but more pronounced. We therefore asked whether Stn1 exerts its effect independently of POT1b. Whereas Stn1 depletion with shRNA in POT1b-proficient cells showed the expected ~2-fold increase in the overhang signal, no increase was observed in POT1b-deficient cells (Figure 4G and Figures S4D and S4E), suggesting that Stn1 depends on POT1b to restore the overhang size.

CST Interacts with POT1b

Consistent with the finding that the effect of Stn1 depends on POT1b (Figure 4G and Figure S4E), a robust interaction between CST and POT1b was observed in coimmunoprecipitation (co-IP) experiments (Figure 5A and Figures S5A–S5C). In contrast, co-IP experiments revealed no interaction of CST with TRF1, TRF2, Rap1, TIN2, and POT1a (Figure S5A–S5C). CST showed a weak interaction with mouse TPP1 in some experiments (Figure S5A), consistent with a report on the binding of human TPP1 to CST (Wan et al., 2009), but this was not observed in other experiments (Figure S5C), and co-transfection of TPP1 was not required for the interaction of POT1b with CST (Figure S5B). All three members of the CST complex could be detected in co-IPs with POT1b (Figures S5A and S5B), and conversely IP of CST brought down POT1b (Figure 5A). Both Ctc1 and Stn1 appeared to be required for the interaction of CST with POT1b, whereas Ten1 was not required for the interaction of POT1b with Ctc1 and Stn1 (Figure S5D).

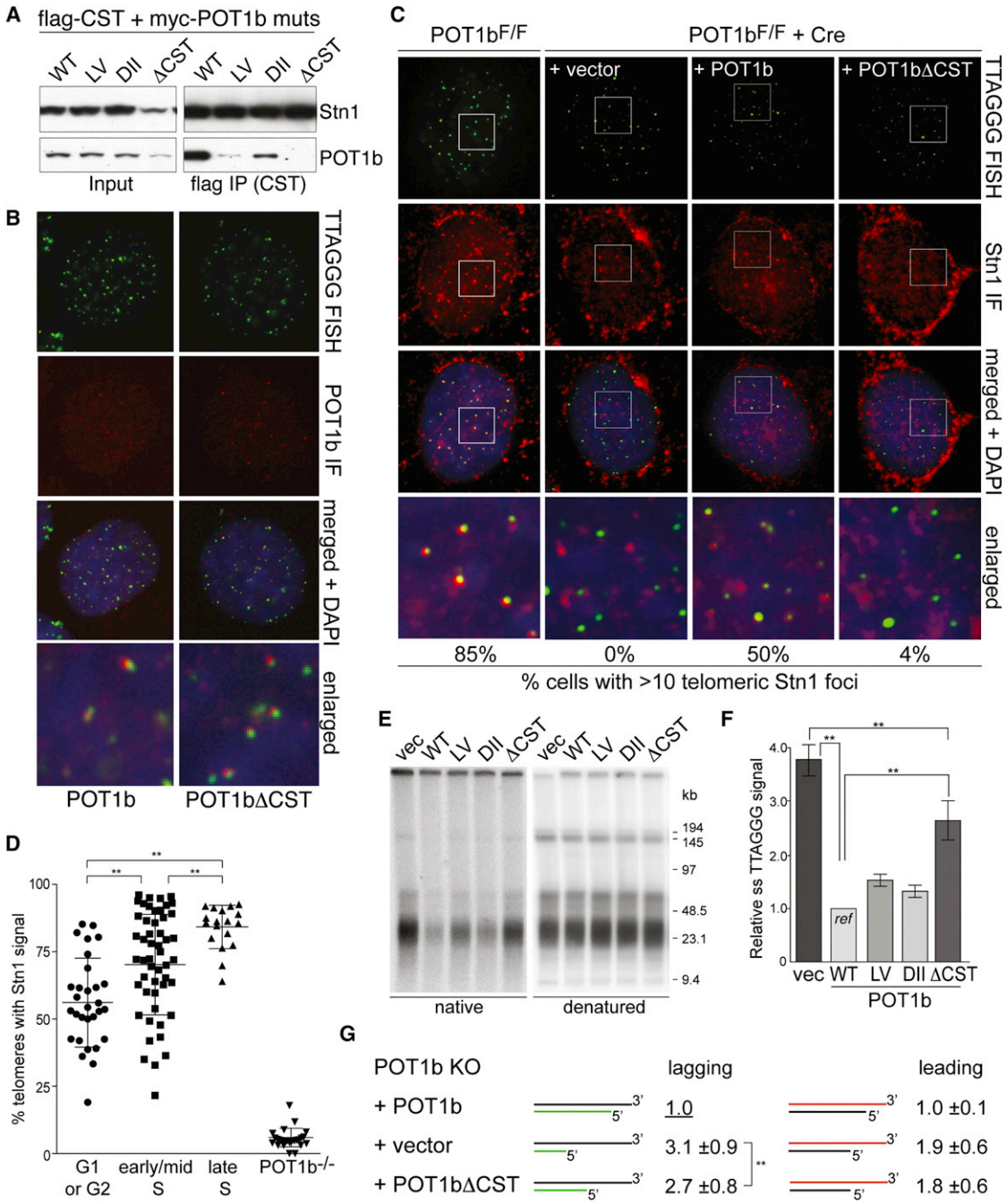

Figure 5. The Telomeric Function of CST Requires Its Interaction with POT1b

(A) Coimmunoprecipitation of POT1b mutants with CST from 293T cells transfected with myc-POT1b alleles and flag-tagged mouse Ctc1, Stn1, and Ten1. FLAG IPs were immunoblotted with FLAG (top) and myc (bottom) Abs.

(B) Telomeric localization of POT1b alleles detected by myc IF (red) in POT1b$^{F/-}$ MEFs after deletion of endogenous POT1b with Cre. Telomeres detected by FISH (C-rich probe, green).

(C) IF-FISH for colocalization of Stn1 with telomeres in POT1b$^{F/F}$ MEFs (left) and in the same cells expressing the indicated POT1b alleles or vector control, after deletion of endogenous POT1b with Cre. Stn1 (red) was detected with an anti-mStn1 antibody. Telomeres (green) are detected by FISH. Cells with 10 or more mStn1 signals colocalizing with telomeres were scored (bottom) (n > 100 nuclei).

(D) Quantification of the telomeric localization of Stn1 at different cell-cycle phases. Each plotted value represents the percentage of telomeres in an individual cell that contain Stn1 signal detected by IF (n > 100 cells). Mean and SDs are shown; ** indicates $p < 0.05$. Cell-cycle phases were determined based on BrdU IF pattern.

(E and F) Overhang analysis of POT1b$^{F/-}$ MEFs expressing the indicated POT1b alleles at 120 hr after Cre. See Figure 1 for details.

(G) Relative overhang size of separated leading- and lagging-end telomeres from POT1b$^{F/-}$ MEFs expressing vector control, wild-type POT1b, or POT1bΔCST, after deletion of endogenous POT1b with Cre. Mean values and SDs of four independent experiments. See also Figures S5 and S6.

We next analyzed the POT1b-CST interaction with the objective of creating a mutant of POT1b defective in CST binding. The region(s) in POT1b required for binding to CST were mapped by using previously characterized chimeras between human POT1 and mouse POT1a and -b (Palm et al., 2009). Co-IPs of the chimeric POT1 proteins and CST indicated that the interaction involved aa 300–350 of POT1b, which is one of two regions in POT1b required for 3′ overhang control (Figures S5E and S5F). However, aa 300–535 of POT1b were not sufficient to confer the CST interaction to POT1a, indicating an additional interaction site near the C terminus of POT1b. Therefore, residues within aa 300–350 and 535–640 in POT1b were mutated to the equivalent POT1a residues (Figure 5A and Figures S5G–S5I). Two mutations in POT1b, L329P/V332E and D638N/I639V/I640V, weakened the interaction with CST (Figures S5G–S5I) while mutating all five residues in POT1b, resulting in a mutant we refer to as POT1bΔCST, completely abolished CST binding (Figure 5A and Figures S6A–S6E). POT1bΔCST retained its ability to bind TPP1, was expressed at the same level as wild-type POT1b, and showed the same subcellular fractionation (Figures S6B–S6D). Importantly, POT1bΔCST was detected at telomeres similar to wild-type POT1b, although the staining for both proteins was weak and only detectable in ~40% of the cells (Figure 5B).

POT1b-Mediated Recruitment Is Required for Overhang Regulation by CST

In the presence of wild-type POT1b, ~85% of cells contained >10 Stn1 foci that colocalized with telomeres (Figure 5C). The percentage of telomeres containing Stn1 foci was significantly increased in late S phase (Figure 5D). However, in cells lacking POT1b or expressing POT1bΔCST, the telomeric localization of Stn1 was strongly reduced (Figures 5C and 5D), even though the POT1bΔCST protein was expressed at the same level as wild-type POT1b (Figure S6B) and localized to telomeres (Figure 5B). These results argue that the interaction with POT1b is the primary mechanism by which CST localizes to telomeres.

Importantly, although wild-type POT1b completely abolishes the 3- to 4-fold excess overhang signal associated with POT1b deletion, in the presence of POT1bΔCST, the telomeric overhang signal remained elevated by ~2 fold (Figures 5E and 5F and Figure S6F). POT1bΔCST affected the overhangs at both newly synthesized telomeres (Figure 5G and Figure S6G), consistent with the results obtained with Stn1 shRNA. In the presence of POT1bΔCST, the overhangs at both leading- and lagging-end telomeres were increased by ~2-fold compared to those in the presence of wild-type POT1b (Figure 5G and Figure S6H). Similar results were obtained when POT1bΔCST was expressed in $POT1b^{-/-}mTR^{-/-}$ cells (Figure S6I). These data argue that the role of CST in limiting overhang size depends on its recruitment by POT1b and is independent of telomerase.

Although the POT1bΔCST mutant mimicked the depletion of Stn1, the elevated overhang signal observed in the absence of POT1b could not be attributed entirely to compromised CST function as POT1b KO cells had overhangs signals that were 1.5-fold greater than in cells expressing POT1bΔCST (Figures 5E and 5F). Furthermore, the overhang signals at lagging-end telomeres in cells lacking POT1b were significantly greater than those in cells expressing POT1bΔCST (Figure 5G), indicating that POT1b was fulfilling a CST-independent function at the lagging-end telomeres.

POT1b Blocks Apollo from Hyperresecting Lagging- and Leading-End Telomeres

Because the data pointed to a CST-independent role of POT1b, we asked whether POT1b protects the C-rich strand from excessive degradation by Apollo using $Apollo^{F/F}POT1b^{F/F}$ MEFs from which Apollo and POT1b could be codeleted with Cre (Figure 6 and Figures S7A and S7B). The increase in overhang signal observed following Cre treatment was substantially attenuated in $Apollo^{F/F}POT1b^{F/F}$ compared to $POT1b^{F/F}$ MEFs (Figures 6A and 6B). Exogenous Apollo reversed the overhang phenotype in Cre-treated $Apollo^{F/F}POT1b^{F/F}$ cells to that associated with deletion of POT1b alone, whereas expression of an Apollo mutant (ApolloΔTRF2 (Wu et al., 2010)) that is unable to localize to telomeres had no effect (Figures S7C and S7D). Importantly, the overhang signal in Apollo/POT1b DKO cells expressing the POT1bΔCST mutant was not significantly different from that in cells with the vector control (Figures 6C and 6D). This result indicated that, in the absence of Apollo, POT1b regulates overhang length primarily through CST.

To determine whether POT1b inhibits Apollo at both newly synthesized telomeres, the leading- and lagging-end telomeres were separated following deletion of Apollo and POT1b (Figures S7E and S7F). At lagging-end telomeres the overhang signal was increased by approximately 2-fold in the Apollo/POT1b DKO setting compared to wild-type (Figures 6E and 6F), which is less of an increase than observed after deletion of POT1b alone (Figures 6F and 4F). Thus, POT1b limits overhang size at lagging-end telomeres in part through the inhibition of Apollo. Meanwhile, the absence of Apollo completely abolished the effect of POT1b deletion on the overhangs of leading-end telomeres. Instead of a ~2 fold increase as in POT1b KO cells, the leading-end telomeres in the Apollo/POT1b DKO cells showed a ~30%–40% reduction in overhang signal compared to wild-type (Figures 6E and 6F), indicating that at leading-end telomeres, the increase in overhang signal induced by POT1b deletion is mediated by Apollo. Consistent with the reduced overhang signal at leading-end telomeres, approximately 10% of chromosomes in Apollo/POT1b DKO cells were engaged in leading-end fusions (Figure S6G). Thus, POT1b inhibits excessive resection by Apollo at both leading- and lagging-end telomeres.

Combinatorial Action of POT1b, Apollo, and Exo1

The data above indicate that POT1b has two functions at telomeres: it inhibits excessive resection by Apollo and recruits CST. As the CST complex primarily functions to correct to extended overhangs generated by Exo1, it is expected that the deletion of POT1b from Exo1-deficient cells will have no effect on this aspect of overhang processing. However, because POT1b also functions to block excessive resection by Apollo, the test of this prediction must be performed in an Apollo-deficient setting. We therefore generated $Apollo^{F/F}POT1b^{F/F}$ MEFs with and without Exo1 and assayed the telomeric overhang following codeletion of Apollo and POT1b with Cre

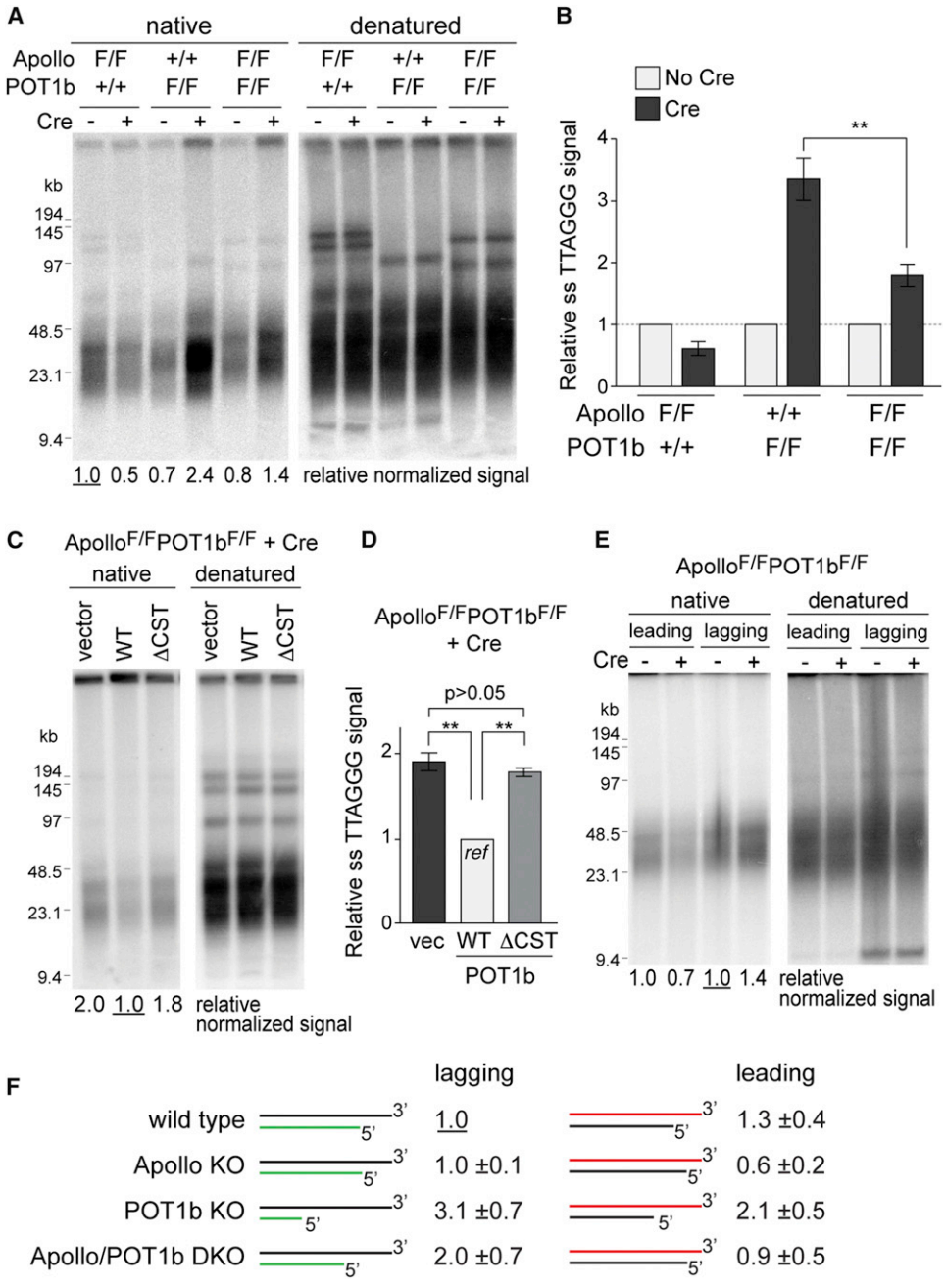

Figure 6. POT1b Inhibits Hyperresection by Apollo

(A and B) Overhang analysis of Apollo$^{F/F}$, POT1b$^{F/F}$, and Apollo$^{F/F}$POT1b$^{F/F}$ MEFs without and at 120 hr after Hit&Run Cre. See Figure 1 for details.

(C and D) Overhang analysis of Apollo$^{F/F}$POT1b$^{F/F}$ MEFs expressing the indicated POT1b alleles at 120 hr after Cre.

(E) Overhang analysis of the leading- and lagging-end telomeres from Apollo$^{F/F}$POT1b$^{F/F}$ MEFs in the absence of Cre and at 120 hr post-Cre.

(F) Relative overhang size in different genetic backgrounds. Values for Apollo/POT1b DKO cells are the mean and SDs of three independent experiments (see Figures 2J, 3F and 5G for data on Apollo KO and POT1b KO). See also Figure S7.

(Figures 7A and 7B). As predicted, the deletion of POT1b from Exo1-deficient cells that also lack Apollo resulted in an overhang signal that was not significantly different from that of wild-type cells containing all three factors (Figures 7A and 7B). These data define the role of POT1b-recruited CST as correcting the extended overhang generated in S phase and Exo1 as the primary source of these excessive overhangs. Furthermore, the data describe the dual role of POT1b in overhang regulation. POT1b recruits CST and thereby ensures the correction of the overhangs generated by Exo1. In addition, POT1b inhibits

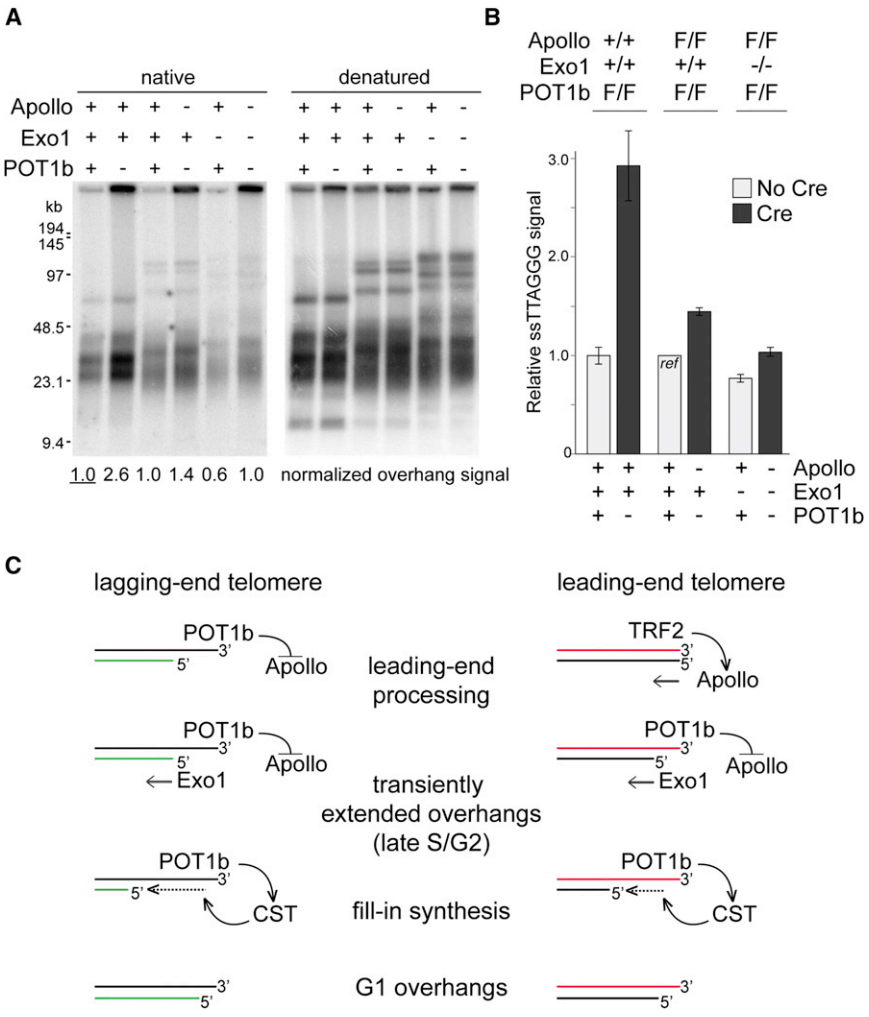

Figure 7. Combinatorial Action of Apollo, Exo1, CST, and POT1b

(A) Overhang assay on Apollo$^{F/F}$POT1b$^{F/F}$ and Apollo$^{F/F}$Exo1$^{-/-}$POT1b$^{F/F}$ MEFs at 96 hr after Hit&Run Cre.

(B) Quantification of overhang analysis in (A). Mean and SDs of three independent experiments. Genotypes of the MEFs (top) and status of each gene (bottom) are indicated.

(C) Model for the generation of the telomeric overhang. Apollo, recruited by TRF2, initiates overhang generation at leading-end telomeres, whereas at lagging-end telomeres an overhang originates from incomplete lagging-strand DNA synthesis. POT1b loaded on the terminal overhang inhibits resection by Apollo at the lagging-end telomere and limits resection by Apollo at leading-end telomeres once Apollo has generated a POT1b binding site. Exo1 acts on both ends to generate transiently elongated overhangs. POT1b then recruits CST, which facilitates fill-in synthesis of the C-rich strand at both ends.

inappropriate processing of the leading- and lagging-end telomeres by Apollo (Figure 7C).

DISCUSSION

How Shelterin Orchestrates Telomere End Processing

These data establish the mechanism by which the 3′ telomeric overhang is generated and illuminate how shelterin controls this process (Figure 7C). The generation of the overhang critically depends on factors involved in DNA replication and repair, including the Apollo/SNM1B nuclease, which initiates overhang formation at leading-end telomeres; Exo1, which transiently elongates overhangs at all telomeres through 5′ end resection in S/G2; and CST/AAF, a DNA polα.primase accessory factor needed to restore the elongated overhangs to their G1 size.

Within shelterin, TRF2 and POT1b are the main players in orchestrating postreplicative telomere end processing. The primary role of TRF2 is to recruit Apollo and thus ensure correct formation of the overhang at all leading-end telomeres. When Apollo is absent, the overhang signal at leading-end telomeres is severely reduced and at least some of the leading-end telomeres fail to protect the chromosome ends. Because TRF2 binds to double-stranded telomeric DNA and has a preference for DNA ends in vitro, it seems well suited to position Apollo at or near the leading-end telomere terminus. Whereas TRF2 mediates the telomeric localization of Apollo, POT1b acts as its negative regulator, ensuring that Apollo's action is limited. POT1b may not be active as a regulator of end processing when telomere ends are blunt. Although POT1b can bind to the TRF1/TIN2/TRF2 complex on the duplex telomeric DNA, we imagine that its binding to ss TTAGGG repeats is required for POT1b to inhibit Apollo. Therefore, at the leading-end telomeres, resection by Apollo may first have to generate a POT1b binding site before POT1b can block further resection by Apollo. At the other sister telomere, however, POT1b should be able to bind immediately to the overhang resulting from lagging-strand DNA synthesis and inhibit Apollo without requirement for initial resection.

In addition to regulating Apollo at both telomere ends, POT1b contributes to telomere end processing through CST. The interaction with CST is specific to POT1b, explaining why POT1a lacks the ability to regulate the telomeric overhang. CST is crucial for the correction of the extended overhangs generated by Exo1 and its recruitment by POT1b ensures the efficiency of this process. As CST interacts with the DNA polα.primase complex, it is also expected to arrive at the telomere with the replication fork. However, recruitment by POT1b may be necessary as CST presumably acts after DNA replication has been completed.

Telomere End Processing by the Apollo and Exo1: Comparison to DSB Processing

According to this data, Apollo and Exo1 are the main nucleases acting on telomeres after DNA replication. Although Apollo/Exo1 DKO cells do show a residual overhang signal, some ss telomeric DNA is expected to arise from lagging-strand synthesis. In addition, nucleolytic activities that are activated by the DNA damage response may be operational at telomeres lacking Apollo because a subset of telomeres in Apollo-deficient cells activate the ATM kinase signaling pathway.

The combined action of Apollo and Exo1 at leading-end telomeres is remarkable because one might have anticipated that leading-end telomeres (and perhaps also lagging-end telomeres) are processed in the same way as DSBs. However, the DNA damage response, including the ATM kinase and the MRN complex, which facilitates CtIP-mediated 5′ end resection at DSBs, does not appear to have a prominent role at wild-type mouse telomeres. Indeed, deficiency in either ATM or Nbs1 is not accompanied by an overhang defect or other telomere dysfunction phenotypes (Dimitrova and de Lange, 2009; Celli and de Lange, 2005; Deng et al., 2009; Attwooll et al., 2009) and our data did not reveal a role in telomere-end processing for the BLM helicase, which has been implicated in DSB resection in yeast and mammalian cells.

Transient Elongation of the Telomeric Overhangs

Exo1 appears to be involved in a futile step that creates transiently elongated overhangs, which are later reset by CST-dependent fill-in synthesis. The lack of an obvious defect in telomere protection in the absence of Exo1 indicates that a protective telomere structure can be formed without it. Furthermore, Exo1 has no net effect on the loss of terminal sequences due to telomere end processing because Exo1 deficiency does not alter the rate of telomere shortening in telomerase-deficient cells. What then might be the purpose of the transient elongation of the overhangs at leading- and lagging-end telomeres? On the one hand, Exo1 action at telomere ends may be a fail-safe mechanism. By allowing Exo1 to resect the 5′ ends without interference by shelterin, overhangs could be generated at every daughter telomere, even if other systems fail. An interesting additional possibility is that the transient long overhangs generated by Exo1 ensure that all telomeres can be elongated by telomerase.

The Role of CST at Mammalian Telomeres

The Cdc13 component of budding yeast CST was first identified based on the cell-cycle arrest induced by deprotected telomeres (Garvik et al., 1995). Budding yeast CST was subsequently shown to protect telomeres from excessive 5′ resection, promote the recruitment of telomerase, and act as a negative regulator of telomere length (reviewed in Bertuch and Lundblad, 2006; Price et al., 2010). Similarly, in fission yeast, CST is crucial for the maintenance of the telomeric DNA, perhaps facilitating its semiconservative replication. By comparison, the protective role described here for mammalian CST is much less pronounced and some of the functions of CST in yeast are relegated to shelterin. However, both yeast and mammalian CST interacts with DNA polymerase α (Goulian et al., 1990; Casteel et al., 2009; Grossi et al., 2004; Qi and Zakian, 2000), and our data suggest that this is the key feature relevant to overhang regulation at mammalian telomeres.

How CST is regulated remains to be determined. Apart from the recruitment of CST by POT1b, it is anticipated that the fill-in synthesis mediated by CST is subject to control because although CST corrects the overhangs, it does not remove them altogether. It is possible that the remaining overhang is due to an intrinsic aspect of this type of fill-in synthesis. On the other hand, a regulatory step could explain the precise ATC-5′ ends of the C-rich telomeric strand (Sfeir et al., 2005).

Implications for the Mechanism of Telomere Attrition

The elucidation of multiple regulatory mechanisms that govern the proper terminal structure of mammalian telomeres is hoped to provide information that may someday guide the treatment of human diseases in which the status of telomere function modifies pathogenesis or prognosis. Because telomere attrition is largely due to telomere end processing, it has been of interest to understand the details of this process and perhaps to identify means of altering the rate of telomere shortening. A slower rate of telomere shortening is predicted to extend the life span of primary human cells with potential clinical implications. On the other hand, more rapid telomere attrition could synergize with the targeting of telomerase in cancer treatment. Our data reveal that the generation of the telomeric overhang in mammalian cells is a complex process involving at least two shelterin proteins and three DNA processing factors, resulting in highly regulated steps as well as redundancies. Although the results do not nominate a single nuclease whose inhibition or activation is predicted to alter telomere attrition rates, POT1b has emerged as a discrete regulatory node with strong effects on telomere dynamics. The translation of this insight into human telomere biology will be a challenge because the single POT1 protein in human cells incorporates functions of both POT1a and POT1b that will need to be deconvolved. Indeed, the great advantage of mouse telomeres has been that the regulation of the telomeric overhang by POT1b can be dissected separately from the repression of ATR kinase signaling by POT1a. This evolutionary oddity has revealed aspects of telomere biology that remain opaque in human cells.

EXPERIMENTAL PROCEDURES

Genetically Altered MEFs

Genetically altered mice harboring Apollo, mTR, Exo1, POT1b, NBS1, BLM, and Rosa26-Cre-ER^{T2} targeted alleles were described previously. See Extended Experimental Procedures for details. MEFs were derived and immortalized with SV40-LT by using standard procedures. For synchronization of primary MEFs in G0, primary MEFs were grown to confluency on 10 cm dishes in DMEM/10% FBS. Medium was changed daily according to the following serum withdrawal protocol: 10% FBS (day 1), 5% FBS (day 2–3), 1% FBS (day 4–5), 0.5% FBS (from day 6 on). FACS analysis showed that the cells were in G0 on day 8.

For introduction of Cre recombinase MEFs were infected four times at 12 hr intervals with pMMP Hit&Run Cre retrovirus. Mock infection was used as a negative control. No selection was applied. Experimental time points were counted as hours or days with t = 0 set at 12 hr after the first infection. For long-term analyses requiring selectable Cre expression, retroviral infection

of pWzl-hygro-Cre or empty vector, as a negative control, was performed, followed by selection with hygromycin. For tamoxifen-inducible Cre-ER system (Rosa26-Cre-ER^{T2}), cells in 10 cm dishes were treated for 6–12 hr with 500 nM 4-OH tamoxifen (Sigma). Cells were washed with PBS and media was replaced. Experimental time points were counted as hours from the time of media change.

Separation of Leading- and Lagging-End Telomeres

MEFs were cultured in the presence of 100 μM of BrdU for 16 hr and then processed with minimal exposure to light. Cells were harvested, and genomic DNA was extracted by phenol-chloroform, precipitated with isopropanol in the presence of 0.2 M sodium acetate (pH 5.5), and resuspended in TE (10 mM Tris, 1 mM EDTA [pH 8.0]); 250 μg DNA was digested overnight with 200 U *MboI* and 200 U *AluI* in 300 μl and loaded onto 5 ml CsCl (final density of 1,800 mg/ml). Samples were ultracentrifuged at 55,000 rpm for 20 hr at 25°C. 100 μl fractions were collected from the bottom of the tube. Aliquots of DNA from each fraction were denatured in 0.1 M NaOH for 20–30 min at 37°C. An equal volume of 12xSSC was added to neutralize the samples. Samples were loaded on a Minifold II Slot Blot (Schleicher and Schuell) onto Hybond-N+ nylon transfer membrane (GE Healthcare/Amersham). The membrane was washed twice with 20xSSC, dried, and baked for 2 hr at 80°C. The membrane was prehybridized at 55°C with Church mix (0.5 M Na phosphate buffer [pH 7.2], 1 mM EDTA, 7% w/v SDS, 1% w/v BSA), and hybridized at 55°C with a ^{32}P-[TTAGGG]$_4$ probe in Church mix. The membrane was washed three times with 4xSSC for 30 min each, once with 4xSSC/0.1% SDS, and exposed to a PhosphorImager screen. Pooled DNA from each peak was then surface dialyzed by rocking the solution on a layer of 2% agarose in a 50 ml tube for 30 min at room temperature to reduce the CsCl concentration. The DNA was ethanol precipitated and resuspended in TE (10 mM Tris-HCl [pH 8.0], 1 mM EDTA).

Analysis of Telomeric DNA by In Gel Hybridization

For the analysis of mouse genomic DNA, cells were suspended in PBS and mixed 1:1 (v/v) with 2% agarose (SeaKem) in PBS to obtain between 5 × 10^5 to 1 × 10^6 cells per plug. Plugs were digested overnight with 1 mg/ml Proteinase K (in 10 mM Tris-HCl [pH 8.0], 250 mM EDTA, 0.2% sodium deoxycholate, 1% sodium lauryl sarcosine), washed four times for 1 hr each with TE, with 1 mM PMSF in the last wash. Plugs were washed once more with H_2O and digestion buffer. Plugs were incubated overnight at 37°C with 60 U *MboI*. The following day, the plugs were washed once in TE, and once in 0.5xTBE, and loaded onto a 1% agarose/0.5xTBE gel. Samples were run for 18–24 hr on a CHEF-DRII PFGE apparatus (BioRad) in 0.5xTBE. The settings were as follows: initial pulse, 5 s; final pulse, 5 s; 6 V/cm; 14°C. The gels were dried and prehybridized in Church mix for 1 hr at 50°C. Hybridization was performed overnight at 50°C in Church mix with 50 ng of γ-^{32}P-ATP end-labeled [AACCCT]$_4$. The gel was washed at 55°C three times for 30 min each in 4xSSC, once for 30 min in 4x SSC/0.1% SDS, and exposed to a PhosphoImager screen overnight. After the image was captured, the gel was denatured in 0.5 M NaOH, 1.5 M NaCl for 30 min, neutralized with two 15 min washes in 0.5 M Tris-HCl pH 7.5, 3 M NaCl, prehybridized in Church mix for 1 hr at 55°C, and hybridized overnight with the same probe at 55°C. The gel was washed and exposed as above. The ss G-rich overhang signal in the native gel was quantified with ImageQuant software and normalized to the total telomeric DNA quantified after the gel had been denatured and rehybridized with the telomeric probe.

FUCCI-FACS Sorting

MEFs were transduced with three infections of mKO2-Cdt1 30/120 (lentiviral) followed by three infections of mAG-Geminin 1/110 (lentiviral) (gifts from A. Miyawaki, [Sakaue-Sawano et al., 2008]) at 6 hr intervals. Cdt1$^+$Gem$^+$ cells were collected by FACS, replated, and infected with two rounds of Hit&Run Cre as appropriate. Sorting of G1 and S phase cells according to levels of Cdt1 and Geminin was performed on BD FACSAria cell sorters (BD Biosciences) with excitation by the 488 nm and 561 nm lasers. Cells were collected in PBS and immediately plated on coverslips or embedded in agarose for DNA analysis.

SUPPLEMENTAL INFORMATION

Supplemental Information includes Extended Experimental Procedures and seven figures and can be found with this article online at http://dx.doi.org/10.1016/j.cell.2012.05.026.

ACKNOWLEDGMENTS

We are thankful to W. Wright, J. Shay, Y. Zhao, and T. Chow at UTSW in Dallas for teaching one of us (P.W.) how to separate leading- and lagging-end telomeres. We thank D. White for expert mouse husbandry and the RU Flow Cytometry Resource Center for help with FACS sorting. De Lange lab members are thanked for advice. P.W. was supported by the NIA/NIH Ruth L. Kirschstein NRSA Individual Fellowship F30AG034744 and NIH MSTP grant GM07739 to the Weill Cornell/RU/MSKCC Tri-Institutional MD-PhD Program. H.T. was supported by a grant from the Breast Cancer Research Foundation. TdL is an American Cancer Society Research Professor. This work was supported by a grant from the NIH (CA076027).

Received: October 31, 2011
Revised: March 12, 2012
Accepted: May 1, 2012
Published online: June 28, 2012

REFERENCES

Artandi, S.E., and DePinho, R.A. (2010). Telomeres and telomerase in cancer. Carcinogenesis *31*, 9–18.

Attwooll, C.L., Akpinar, M., and Petrini, J.H. (2009). The mre11 complex and the response to dysfunctional telomeres. Mol. Cell. Biol. *29*, 5540–5551.

Bae, J.B., Mukhopadhyay, S.S., Liu, L., Zhang, N., Tan, J., Akhter, S., Liu, X., Shen, X., Li, L., and Legerski, R.J. (2008). Snm1B/Apollo mediates replication fork collapse and S Phase checkpoint activation in response to DNA interstrand cross-links. Oncogene *27*, 5045–5056.

Bertuch, A.A., and Lundblad, V. (2006). The maintenance and masking of chromosome termini. Curr. Opin. Cell Biol. *18*, 247–253.

Casteel, D.E., Zhuang, S., Zeng, Y., Perrino, F.W., Boss, G.R., Goulian, M., and Pilz, R.B. (2009). A DNA polymerase-alphamiddle dotprimase cofactor with homology to replication protein A-32 regulates DNA replication in mammalian cells. J. Biol. Chem. *284*, 5807–5818.

Celli, G.B., and de Lange, T. (2005). DNA processing is not required for ATM-mediated telomere damage response after TRF2 deletion. Nat. Cell Biol. *7*, 712–718.

Chai, W., Du, Q., Shay, J.W., and Wright, W.E. (2006). Human telomeres have different overhang sizes at leading versus lagging strands. Mol. Cell *21*, 427–435.

Chen, Y., Yang, Y., van Overbeek, M., Donigian, J.R., Baciu, P., de Lange, T., and Lei, M. (2008). A shared docking motif in TRF1 and TRF2 used for differential recruitment of telomeric proteins. Science *319*, 1092–1096.

Dai, X., Huang, C., Bhusari, A., Sampathi, S., Schubert, K., and Chai, W. (2010). Molecular steps of G-overhang generation at human telomeres and its function in chromosome end protection. EMBO J. *29*, 2788–2801.

Denchi, E.L., and de Lange, T. (2007). Protection of telomeres through independent control of ATM and ATR by TRF2 and POT1. Nature *448*, 1068–1071.

Deng, Y., Guo, X., Ferguson, D.O., and Chang, S. (2009). Multiple roles for MRE11 at uncapped telomeres. Nature *460*, 914–918.

Dimitrova, N., and de Lange, T. (2009). Cell cycle dependent role of MRN at dysfunctional telomeres: ATM signaling-dependent induction of NHEJ in G1 and resection-mediated inhibition of NHEJ in G2. Mol. Cell. Biol. *29*, 5552–5563.

Gao, H., Cervantes, R.B., Mandell, E.K., Otero, J.H., and Lundblad, V. (2007). RPA-like proteins mediate yeast telomere function. Nat. Struct. Mol. Biol. *14*, 208–214.

Garvik, B., Carson, M., and Hartwell, L. (1995). Single-stranded DNA arising at telomeres in cdc13 mutants may constitute a specific signal for the RAD9 checkpoint. Mol. Cell. Biol. *15*, 6128–6138.

Goulian, M., Heard, C.J., and Grimm, S.L. (1990). Purification and properties of an accessory protein for DNA polymerase alpha/primase. J. Biol. Chem. *265*, 13221–13230.

Gravel, S., Chapman, J.R., Magill, C., and Jackson, S.P. (2008). DNA helicases Sgs1 and BLM promote DNA double-strand break resection. Genes Dev. *22*, 2767–2772.

Grossi, S., Puglisi, A., Dmitriev, P.V., Lopes, M., and Shore, D. (2004). Pol12, the B subunit of DNA polymerase alpha, functions in both telomere capping and length regulation. Genes Dev. *18*, 992–1006.

Guo, X., Deng, Y., Lin, Y., Cosme-Blanco, W., Chan, S., He, H., Yuan, G., Brown, E.J., and Chang, S. (2007). Dysfunctional telomeres activate an ATM-ATR-dependent DNA damage response to suppress tumorigenesis. EMBO J. *26*, 4709–4719.

He, H., Wang, Y., Guo, X., Ramchandani, S., Ma, J., Shen, M.F., Garcia, D.A., Deng, Y., Multani, A.S., You, M.J., and Chang, S. (2009). Pot1b deletion and telomerase haploinsufficiency in mice initiate an ATR-dependent DNA damage response and elicit phenotypes resembling dyskeratosis congenita. Mol. Cell. Biol. *29*, 229–240.

Hockemeyer, D., Sfeir, A.J., Shay, J.W., Wright, W.E., and de Lange, T. (2005). POT1 protects telomeres from a transient DNA damage response and determines how human chromosomes end. EMBO J. *24*, 2667–2678.

Hockemeyer, D., Daniels, J.P., Takai, H., and de Lange, T. (2006). Recent expansion of the telomeric complex in rodents: Two distinct POT1 proteins protect mouse telomeres. Cell *126*, 63–77.

Hockemeyer, D., Palm, W., Wang, R.C., Couto, S.S., and de Lange, T. (2008). Engineered telomere degradation models dyskeratosis congenita. Genes Dev. *22*, 1773–1785.

Huffman, K.E., Levene, S.D., Tesmer, V.M., Shay, J.W., and Wright, W.E. (2000). Telomere shortening is proportional to the size of the G-rich telomeric 3′-overhang. J. Biol. Chem. *275*, 19719–19722.

Lam, Y.C., Akhter, S., Gu, P., Ye, J., Poulet, A., Giraud-Panis, M.J., Bailey, S.M., Gilson, E., Legerski, R.J., and Chang, S. (2010). SNMIB/Apollo protects leading-strand telomeres against NHEJ-mediated repair. EMBO J. *29*, 2230–2241.

Lenain, C., Bauwens, S., Amiard, S., Brunori, M., Giraud-Panis, M.J., and Gilson, E. (2006). The Apollo 5′ exonuclease functions together with TRF2 to protect telomeres from DNA repair. Curr. Biol. *16*, 1303–1310.

Longhese, M.P., Bonetti, D., Manfrini, N., and Clerici, M. (2010). Mechanisms and regulation of DNA end resection. EMBO J. *29*, 2864–2874.

Makarov, V.L., Hirose, Y., and Langmore, J.P. (1997). Long G tails at both ends of human chromosomes suggest a C strand degradation mechanism for telomere shortening. Cell *88*, 657–666.

McElligott, R., and Wellinger, R.J. (1997). The terminal DNA structure of mammalian chromosomes. EMBO J. *16*, 3705–3714.

Mimitou, E.P., and Symington, L.S. (2008). Sae2, Exo1 and Sgs1 collaborate in DNA double-strand break processing. Nature *455*, 770–774.

Miyake, Y., Nakamura, M., Nabetani, A., Shimamura, S., Tamura, M., Yonehara, S., Saito, M., and Ishikawa, F. (2009). RPA-like mammalian Ctc1-Stn1-Ten1 complex binds to single-stranded DNA and protects telomeres independently of the Pot1 pathway. Mol. Cell *36*, 193–206.

Ohki, R., and Ishikawa, F. (2004). Telomere-bound TRF1 and TRF2 stall the replication fork at telomeric repeats. Nucleic Acids Res. *32*, 1627–1637.

Palm, W., and de Lange, T. (2008). How shelterin protects mammalian telomeres. Annu. Rev. Genet. *42*, 301–334.

Palm, W., Hockemeyer, D., Kibe, T., and de Lange, T. (2009). Functional dissection of human and mouse POT1 proteins. Mol. Cell. Biol. *29*, 471–482.

Price, C.M., Boltz, K.A., Chaiken, M.F., Stewart, J.A., Beilstein, M.A., and Shippen, D.E. (2010). Evolution of CST function in telomere maintenance. Cell Cycle *9*, 3157–3165.

Qi, H., and Zakian, V.A. (2000). The Saccharomyces telomere-binding protein Cdc13p interacts with both the catalytic subunit of DNA polymerase alpha and the telomerase-associated est1 protein. Genes Dev. *14*, 1777–1788.

Sakaue-Sawano, A., Kurokawa, H., Morimura, T., Hanyu, A., Hama, H., Osawa, H., Kashiwagi, S., Fukami, K., Miyata, T., Miyoshi, H., et al. (2008). Visualizing spatiotemporal dynamics of multicellular cell-cycle progression. Cell *132*, 487–498.

Schaetzlein, S., Kodandaramireddy, N.R., Ju, Z., Lechel, A., Stepczynska, A., Lilli, D.R., Clark, A.B., Rudolph, C., Kuhnel, F., Wei, K., et al. (2007). Exonuclease-1 deletion impairs DNA damage signaling and prolongs lifespan of telomere-dysfunctional mice. Cell *130*, 863–877.

Sfeir, A.J., Chai, W., Shay, J.W., and Wright, W.E. (2005). Telomere-end processing the terminal nucleotides of human chromosomes. Mol. Cell *18*, 131–138.

Surovtseva, Y.V., Churikov, D., Boltz, K.A., Song, X., Lamb, J.C., Warrington, R., Leehy, K., Heacock, M., Price, C.M., and Shippen, D.E. (2009). Conserved telomere maintenance component 1 interacts with STN1 and maintains chromosome ends in higher eukaryotes. Mol. Cell *36*, 207–218.

van Overbeek, M., and de Lange, T. (2006). Apollo, an Artemis-related nuclease, interacts with TRF2 and protects human telomeres in S phase. Curr. Biol. *16*, 1295–1302.

Wan, M., Qin, J., Songyang, Z., and Liu, D. (2009). OB fold-containing protein 1 (OBFC1), a human homolog of yeast Stn1, associates with TPP1 and is implicated in telomere length regulation. J. Biol. Chem. *284*, 26725–26731.

Wu, L., Multani, A.S., He, H., Cosme-Blanco, W., Deng, Y., Deng, J.M., Bachilo, O., Pathak, S., Tahara, H., Bailey, S.M., et al. (2006). Pot1 deficiency initiates DNA damage checkpoint activation and aberrant homologous recombination at telomeres. Cell *126*, 49–62.

Wu, P., van Overbeek, M., Rooney, S., and de Lange, T. (2010). Apollo contributes to G overhang maintenance and protects leading-end telomeres. Mol. Cell *39*, 606–617.

Zhu, Z., Chung, W.H., Shim, E.Y., Lee, S.E., and Ira, G. (2008). Sgs1 helicase and two nucleases Dna2 and Exo1 resect DNA double-strand break ends. Cell *134*, 981–994.

Cell

EXTENDED EXPERIMENTAL PROCEDURES

Genetically Altered MEFs and Cell Culture

Mice harboring Apollo, mTR, Exo1, POT1b, NBS1, BLM, and Rosa26-Cre-ER^{T2} targeted alleles were described previously (Ventura et al., 2007; Blasco et al., 1997; Wu et al., 2010; Wei et al., 2003; Chester et al., 1998; Hockemeyer et al., 2006; Reina-San-Martin et al., 2005). Compound genotypes were created by intercrosses and mouse embryonic fibroblasts (MEFs) were obtained from E13.5 embryos by using standard techniques and cultured in DMEM (GIBCO) supplemented with 15% fetal bovine serum (GIBCO), 2 mM L-glutamine, 100 U/ml penicillin (Sigma), 0.1 μg/ml streptomycin (Sigma), 0.1 mM nonessential amino acids (Invitrogen), 1 mM sodium pyruvate (Sigma), and 50 μM β-mercaptoethanol (Chemicon). Primary MEFs were immortalized at passage 2 with pBabe SV40-LT (gift from G. Hannon) by retroviral transduction. SV40-LT immortalized cells, the Phoenix ecotropic packaging cell line (ATCC), and 293T cells were grown in DMEM as above with 10% bovine calf serum (Hyclone) and without pyruvate and β-ME.

For synchronization of primary MEFs in G0, primary MEFs were grown to confluency on 10 cm dishes in DMEM/10% FBS. Medium was changed daily according to the following serum withdrawal protocol: 10% FBS (day 1), 5% FBS (day 2-3), 1% FBS (day 4-5), 0.5% FBS (from day 6 on). FACS analysis showed that the cells were in G0 on day 8.

FACS

For cell-cycle analysis, cells were pulsed with 10 μM BrdU for 30 min, fixed, and stained with FITC-conjugated anti-BrdU antibody (BD Biosciences) and PI. Flow cytometry was performed on FACS Calibur-1 (Becton Dickinson), and data were analyzed by using FlowJo software.

Immunoblotting and Immunofluorescence

The anti-mouse Stn1 mouse polyclonal antibody was raised against recombinant GST-full length mouse Stn1. The GST-tag was excised before immunization. Other antibodies used in immunoblots are TRF2 (1254), POT1b (1223), POT1a (1221), Chk2 (611570, BD Biosciences), γ-tubulin (GTU-88, Sigma), myc (9B11, Cell Signaling), FLAG (M2, Sigma), HA (HA.11, Covance), NBS1 (a gift from John Petrini), BLM (ab2179, Abcam), and BrdU (ab6326, Abcam). Cells were lysed in 2xLaemmli buffer (100 mM Tris-HCl at pH 6.8, 200 mM DTT, 3% SDS, 20% glycerol, 0.05% bromophenol blue) at 10^4 cells/μl, denatured for 5 min at 100°C, and sheared with an insulin needle before loading the equivalent of 2×10^5 cells per lane. Protein samples were separated by SDS-PAGE and blotted to nitrocellulose membranes. The membranes were blocked in 5% nonfat dry milk in PBS-T (0.1% Tween-20 in PBS) for 30 min and incubated with primary antibodies in 0.1% or 1% milk in PBS-T at room temperature for at least for 1 hr. Immunoblots for POT1b were performed via the renaturation protocol described previously (Loayza and De Lange, 2003).

Coimmunoprecipitation

4-5 X10^6 293T cells were plated in a 10 cm dish 20-24 hr prior to transfection by calcium-phosphate precipitation method by using 6 μg of each plasmid DNA as indicated. 40 hr later, cells were harvested, rinsed with PBS, resuspended in 0.5 ml lysis buffer (50 mM Tris-HCl (pH 7.4), 150 mM NaCl, 1 mM EDTA, 10% glycerol, 8 mM β-mercaptoethanol, 0.5% NP-40, Complete protease inhibitor mix (Roche), and PhosSTOP phosphatase inhibitor mix (Roche)), and incubated on ice for 1 hr. After centrifugation at 16,000 g for 10 min at 4°C, 1.5 μl of anti-myc antibody (9B11) was added to the supernatant. Samples were nutated at 4°C for 4 hr. 20 μl (bed volume) of a Protein G Sepharose (Amersham) slurry preincubated with 5% BSA/PBS, was added and the sample was nutated at 4°C for an additional hour. Beads were washed 4 times at 4°C with the lysis buffer containing 0.25% NP-40 and immunoprecipitated protein was eluted with 50 μl of 2xLaemmli buffer. Samples were boiled for 5 min before separation on SDS-PAGE.

IF-FISH

Cells grown on coverslips were rinsed with PBS. Prior to fixation, cells were treated for 5 min with Triton X-100 extraction buffer (0.1% Triton X-100, 20 mM HEPES-KOH pH 7.9, 50 mM NaCl, 3 mM $MgCl_2$, 300 mM sucrose) on ice. Extracted cells were fixed with 3% paraformaldehyde/2% sucrose in PBS for 10 min at room temperature (RT), and washed twice with PBS. The cells were blocked with blocking solution (1 mg/ml BSA, 3% goat serum, 0.1% Triton X-100 and 1 mM EDTA pH 8.0 in PBS) for 1 hr at RT. Cells were incubated with primary antibody diluted in blocking solution for 2 hr at RT or overnight at 4°C, washed 3 times with PBS, incubated with secondary antibody in the same solution for 1 hr at RT, and washed 3 times with PBS. Cells were fixed again with 2% paraformaldehyde in PBS for 5 min, dehydrated in 70%, 95%, and 100% ethanol for 5 min each, and allowed to air dry completely. Hybridizing solution (70% formamide, 0.5% (w/v) blocking reagent (Roche), 10 mM Tris-HCl (pH 7.2), containing PNA probe FITC-OO-$[CCCTAA]_3$-3′ (Applied Biosystems) was added to each coverslip and the cells were denatured for 5 min at 80°C on a heat block. After 2 hr incubation at RT in the dark, cells were washed twice with washing solution (70% formamide, 10 mM Tris-HCl [pH 7.2]) for 15 min each and in PBS for three times for 5 min each. To the second PBS wash, 0.1 μg/ml DAPI was added. Coverslips were sealed onto glass slides with embedding media (ProLong Gold Antifade Reagent, Invitrogen).

For BrdU staining, cells were cultured in 10 μM BrdU containing medium for 30 min. Cells were fixed, incubated with primary and secondary antibody and fixed again as described above. Cells were treated with 4N HCl for 3 min, rinsed with PBS and incubated with anti-BrdU antibody and secondary antibody. Cells were fixed again and used for fluorescence in situ hybridization (FISH) as described above. Staging of S-phase cells were done as described previously (Dimitrova and Berezney, 2002).

shRNA

The mouse Stn1 shRNA (GATCCTGTGTTTCTAGCCTTT) and Ctc1 shRNA (CGGCAGATCACAGCATGATAA) were expressed from the pLKO.1 lentivirus (OpenBiosystems).

Apollo, CST, and POT1b Constructs

N-terminal FLAG-[HA]2-tagged ApolloΔTRF2 allele was generated by PCR-mediated mutagenesis as described previously (Wu et al., 2010). N-terminal myc-tagged (N-myc) POT1 chimera constructs (AB, AB2, AH, AH2, HA, HA2, HB, and HB2) were described previously (Palm et al., 2009) and subcloned into pLPC puromycin-selectable retroviral vector. N-myc POT1 chimera constructs (AB2 350, AB2 408, AB2 462, and AB2 535) were generated as below and cloned to pLPC puromycin vector. AB2 350: POT1a(aa 1-301)-POT1b(300-350)-POT1a(350-1920), AB2 408: POT1a(1-301)-POT1b(300-408)-POT1a(408-1920), AB2 462: POT1a(1-301)-POT1b(300-462)-POT1b(462-1920), AB2 535: POT1a(1-301)-POT1b(300-535)-POT1b(535-1920). N-myc POT1b alleles (EAIQ, DDTY, LV, SD, RR, H570H, Q591T, S620I, HQ, SHQ, DII, ΔCST) were generated by QuikChange site-directed mutagenesis (Agilent Technologies) by using N-myc POT1b in pLPC puromycin as template. N-terminal FLAG-tagged mouse Ctc1, Stn1 and Ten1 were cloned into pLPC puromycin vector by PCR cloning using IMAGE ID 9056325, FANTOM3 ID I920076F07, and IMAGE ID 1069092, respectively.

Retroviral Gene Delivery

For infection of mouse cells, 24 hr prior to transfection, $5x10^6$ Phoenix ecotropic packaging cells were plated in 10 cm dishes. Phoenix cells were transfected with 20 μg of the appropriate plasmid DNA by CaPO4 precipitation (described below). The media were refreshed 6-8 hr later. 36 hr after transfection, media were collected and filtered through a 0.45 μm filter. Polybrene was added to a final concentration of 4 μg/mL and the virus-containing medium was used to infected target cells plated 24 hr earlier at a density of 5×10^5 cells per 10 cm dish. Fresh media were added to the virus-producing cells, and the same cells were used for a total of 3-4 infections at 12 hr intervals. 12 hr after the last infection, cells were split into fresh media containing antibiotics for selection, as appropriate (puromycin: 2 μg/ml, hygromycin: 90 μg/ml). Selection was maintained for 3 days in the presence of puromycin or 5 days in the presence of hygromycin, until uninfected control cells had died. Experimental time points were counted as hours or days from t = 0 set at 12 hr after the first infection.

Lentiviral Gene Delivery

24 hr prior to transfection, $5x10^6$ 293T cells were plated in 10 cm dishes. 293T cells were transfected with 10 μg of the appropriate plasmid DNA, along with packaging plasmids (5 μg pVSVg, 3 μg pMDLg, 2.5 μg pRSV) by $CaPO_4$ precipitation. The media were refreshed 6-8 hr later. The first infection was performed at 36 hr after transfection. Target cells were infected for a total of 3-4 infections at 4-6 hr intervals. Experimental time points were counted as hours or days from t = 0 set at 12 hr after the first infection.

Telomere FISH

MEFs were grown to approximately 80% confluence on 10-cm dishes and incubated for 90 min in 0.2 μg/ml colcemide (Sigma). Cells were harvested by trypsinization, centrifuged at 1000 rpm for 5 min, and resuspended in 0.075 M KCl prewarmed to 37°C. Cells were incubated at 37°C for 15-30 min with occasional inversion. Cells were centrifuged at 1000 rpm for 5 min and the supernatant was decanted. 500 μl of cold 3:1 methanol:glacial acetic acid fixative was added dropwise while cells were mixed gently on a vortexer (<1000 rpm). Another 500 μl fixative was added slowly with mixing. Tubes were then filled to 10 ml with fixative and fixed at 4°C for at least 24 hr. To prepare metaphase spreads, cells were centrifuged at 1000 rpm for 5 min and the supernatant was decanted. Cells were resuspended in 1 ml remaining fixative and 100 μl was dropped onto glass slides in a temperature- and humidity-controlled chamber set at 4°C and 50% humidity (Thermotron). Slides were washed with fixative and dried overnight.

For peptide nucleic acid (PNA) FISH, slides were washed in PBS once and fixed in 4% formaldehyde for 2 min at room temperature. After three PBS washes for 5 min each, spreads were digested for 10 min at 37°C with 1 mg/ml pepsin dissolved in 10 mM glycine, pH 2.2. Slides were then washed in PBS, fixed again in 4% formaldehyde for 2 min at room temperature, and washed in PBS before dehydration by 5 min incubation with 70%, 95%, and 100% ethanol. After air-drying, hybridizing solution (70% formamide, 1 mg/ml blocking reagent (Roche), 10 mM Tris-HCl, pH 7.2) containing FITC-OO-$(CCCTAA)_3$ PNA probe (Applied Biosystems) was added, and spreads were denatured by heating for 3 min at 80°C on a heating block. Spreads were then allowed to hybridize in the dark for 2 hr at room temperature or overnight at at 4°C. Two 15 min washes were performed in a mixture containing 70% formamide, 10 mM Tris-HCl, pH 7.2, followed by three washes in a mixture containing 0.1 M Tris, HCl, pH 7.2, 0.15 M NaCl, and 0.08% Tween-20, with DAPI added to the second wash to counter-stain the chromosomal DNA. Slides were mounted in embedding medium (ProLong Gold Antifade Reagent, Invitrogen), and digital images were captured with a Zeiss Axioplan II microscope with a Hamamatsu C4742-95 camera by using Improvision OpenLab software.

Cell Fractionation

Cell fractionation was performed as described (Méndez and Stillman, 2000). Cells were trypsinized, suspended in media containing serum, collected by centrifugation, and washed with PBS. All procedures were performed on ice. Cells were suspended in ice-cold buffer A (10 mM HEPES (pH 7.9), 10 mM KCl, 1.5 mM MgCl, 0.34 M sucrose, 10% glycerol, 1 mM dithiothreitol (DTT), 1 mM PMSF

and a protease inhibitor cocktail). Triton X-100 as added to 0.1% and cells were incubated for 10 min. The cytoplasmic fraction was collected by centrifugation at 1,300 g for 5 min. After washing with buffer A, the cell pellet was suspended in buffer B (3 mM, EDTA, 0.2 mM EGTA, 1 mM DTT and protease inhibitors described above) and incubated for 30 min. The lysate was fractionated to the supernatant (soluble nuclear fraction) and pellet (chromatin fraction) by centrifugation at 1,700 g for 5 min.

SUPPLEMENTAL REFERENCES

Blasco, M.A., Lee, H.W., Hande, M.P., Samper, E., Lansdorp, P.M., DePinho, R.A., and Greider, C.W. (1997). Telomere shortening and tumor formation by mouse cells lacking telomerase RNA. Cell *91*, 25–34.

Chester, N., Kuo, F., Kozak, C., O'Hara, C.D., and Leder, P. (1998). Stage-specific apoptosis, developmental delay, and embryonic lethality in mice homozygous for a targeted disruption in the murine Bloom's syndrome gene. Genes Dev. *12*, 3382–3393.

Dimitrova, D.S., and Berezney, R. (2002). The spatio-temporal organization of DNA replication sites is identical in primary, immortalized and transformed mammalian cells. J. Cell Sci. *115*, 4037–4051.

Hockemeyer, D., Daniels, J.P., Takai, H., and de Lange, T. (2006). Recent expansion of the telomeric complex in rodents: Two distinct POT1 proteins protect mouse telomeres. Cell *126*, 63–77.

Loayza, D., and De Lange, T. (2003). POT1 as a terminal transducer of TRF1 telomere length control. Nature *423*, 1013–1018.

Méndez, J., and Stillman, B. (2000). Chromatin association of human origin recognition complex, cdc6, and minichromosome maintenance proteins during the cell cycle: assembly of prereplication complexes in late mitosis. Mol. Cell. Biol. *20*, 8602–8612.

Palm, W., Hockemeyer, D., Kibe, T., and de Lange, T. (2009). Functional dissection of human and mouse POT1 proteins. Mol. Cell. Biol. *29*, 471–482.

Reina-San-Martin, B., Nussenzweig, M.C., Nussenzweig, A., and Difilippantonio, S. (2005). Genomic instability, endoreduplication, and diminished Ig class-switch recombination in B cells lacking Nbs1. Proc. Natl. Acad. Sci. USA *102*, 1590–1595.

Ventura, A., Kirsch, D.G., McLaughlin, M.E., Tuveson, D.A., Grimm, J., Lintault, L., Newman, J., Reczek, E.E., Weissleder, R., and Jacks, T. (2007). Restoration of p53 function leads to tumour regression in vivo. Nature *445*, 661–665.

Wei, K., Clark, A.B., Wong, E., Kane, M.F., Mazur, D.J., Parris, T., Kolas, N.K., Russell, R., Hou, H.J., Jr., Kneitz, B., et al. (2003). Inactivation of Exonuclease 1 in mice results in DNA mismatch repair defects, increased cancer susceptibility, and male and female sterility. Genes Dev. *17*, 603–614.

Wu, P., van Overbeek, M., Rooney, S., and de Lange, T. (2010). Apollo contributes to G overhang maintenance and protects leading-end telomeres. Mol. Cell *39*, 606–617.

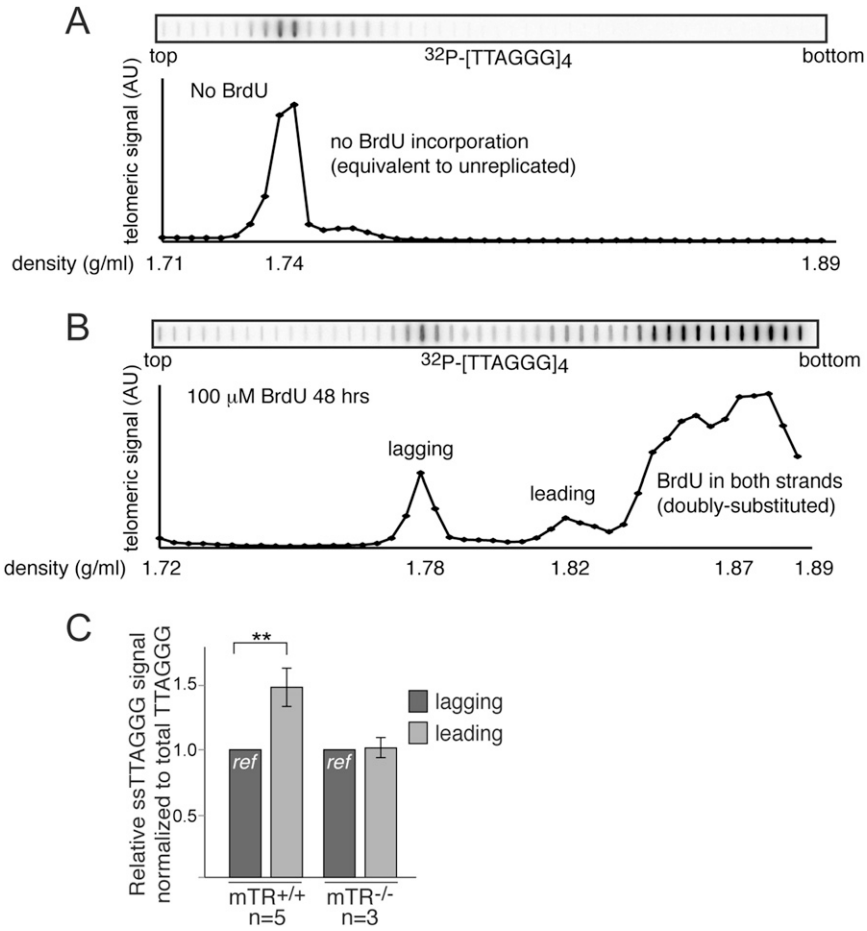

Figure S1. Slot Blots of Telomeric Signals Corresponding to Unreplicated and Doubly-Substituted Telomeric DNA, Related to Figure 1

(A) Slot blot of telomeric signals in fractions collected from a CsCl gradient by using DNA from MEFs not labeled with BrdU. (B) Slot blot of telomeric signals in fractions collected from a CsCl gradient by using telomeric DNA isolated from MEFs incubated for 48 hr (>2 PDs) with BrdU. (C) Quantification of relative overhang signal at lagging- and leading-end telomeres in telomerase-proficient and -deficient MEFs.

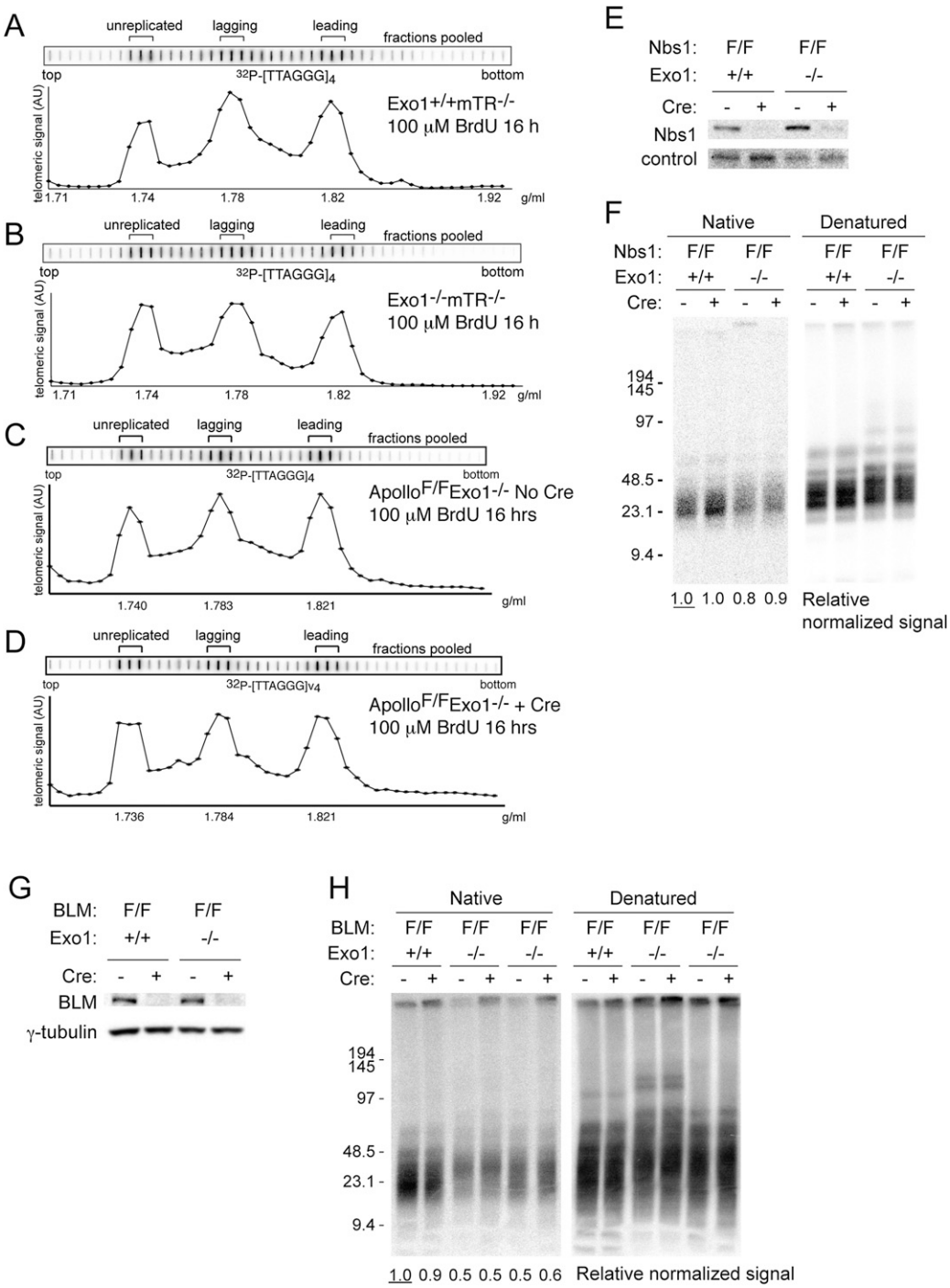

Figure S2. Effects of Exo1, Apollo, Nbs1, and BLM, Related to Figure 2

(A–D) Representative slot blots of telomeric signalS in fractions collected CsCl density gradient equilibrium centrifugation of telomeric DNA from Exo1$^{+/+}$mTR$^{-/-}$ (A), Exo1$^{-/-}$mTR$^{-/-}$ (B), and Apollo$^{F/F}$Exo1$^{-/-}$ MEFs in the absence of Cre (C) and at 120 hr after Hit&Run Cre (D), after labeling with BrdU for one round of replication. The fractions pooled for overhang analyses are shown.

(E) Immunoblot for Nbs1 in Exo1$^{+/+}$Nbs1$^{F/F}$ and Exo1$^{-/-}$Nbs1$^{F/F}$ MEFs without Cre and 120 hr after Hit&Run Cre.

(F) Overhang assay of cells in (E). Relative ss TTAGGG signal in each lane of the native gel was normalized to the total TTAGGG signal in the same lane of the denatured gel, with the value in lane 1 set to 1.

(G) Immunoblot for BLM in Exo1$^{+/+}$BLM$^{F/F}$ and Exo1$^{-/-}$BLM$^{F/F}$ MEFs without Cre and 120 hr after Hit&Run Cre.

(H) Overhang assay of cells in (G). Relative ss TTAGGG signal in each lane of the native gel was normalized to the total TTAGGG signal in the same lane of the denatured gel, with the value in lane 1 set to 1.

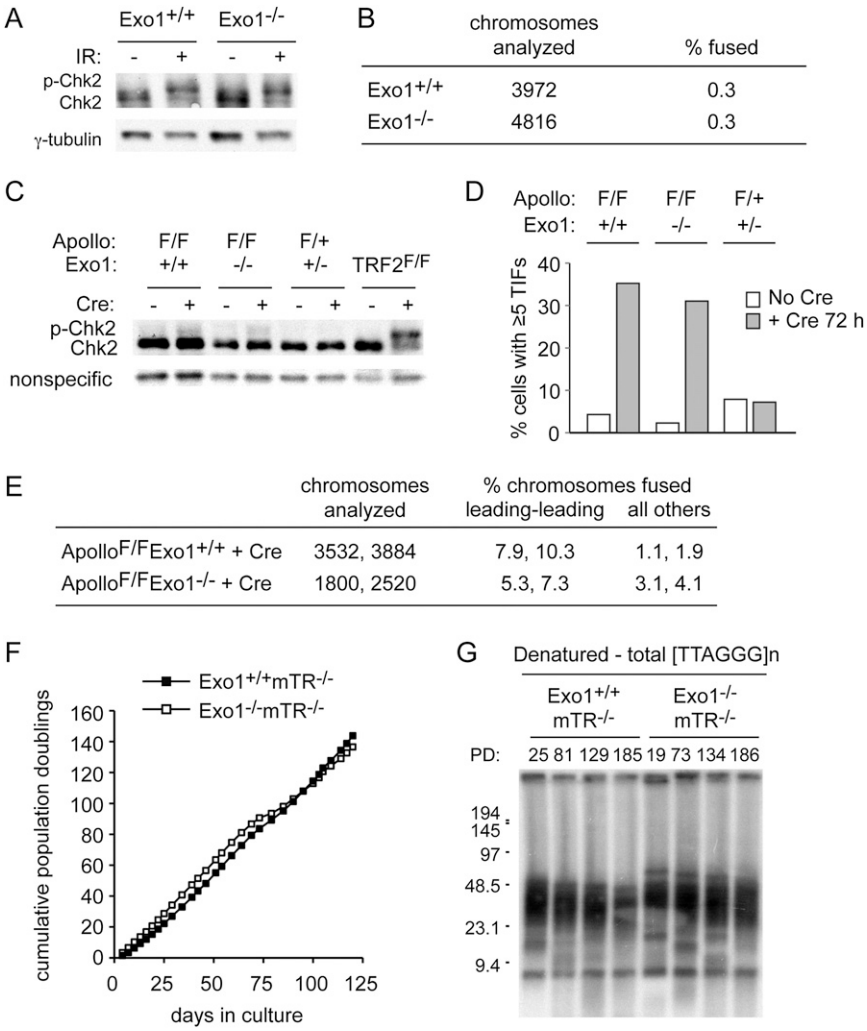

Figure S3. Exo1 Is Not Required for Telomere End Protection, Related to Figure 2

(A) Immunoblot detection of Chk2 phosphorylation status of wild-type and Exo1-deficient MEFs. As a positive control, cells were treated with 2 Gy of γ-irradiation and cultured for 30 min.

(B) Quantification of telomere fusion events on metaphase spreads from Exo1-proficient and -deficient MEFs. Metaphase spreads were obtained from Exo1$^{-/-}$ and Exo1$^{+/+}$ MEFs and processed for telomeric FISH.

(C) Immunoblot detection of Chk2 phosphorylation status of Apollo$^{F/F}$ and Apollo$^{F/F}$Exo1$^{-/-}$ in the absence and presence of Hit&Run Cre.

(D) Quantification of TIFs defined as the colocalization of 53BP1 detected by indirect immunofluorescence with telomeres detected by FISH.

(E) Quantification of CO-FISH analysis detecting telomere fusions in Apollo$^{F/F}$ and Apollo$^{F/F}$Exo1$^{-/-}$ MEFs at 120 hr after Hit&Run Cre.

(F) Growth curve of SV40-LT immortalized Exo1$^{+/+}$mTR$^{-/-}$ and Exo1$^{-/-}$mTR$^{-/-}$ MEFs passaged in parallel for 120 days in culture.

(G) In gel detection of the denatured telomeric signal in DNA from Exo1$^{+/+}$mTR$^{-/-}$ and Exo1$^{-/-}$mTR$^{-/-}$ MEFs harvested after the indicated population doublings, according to the growth curve shown in (F).

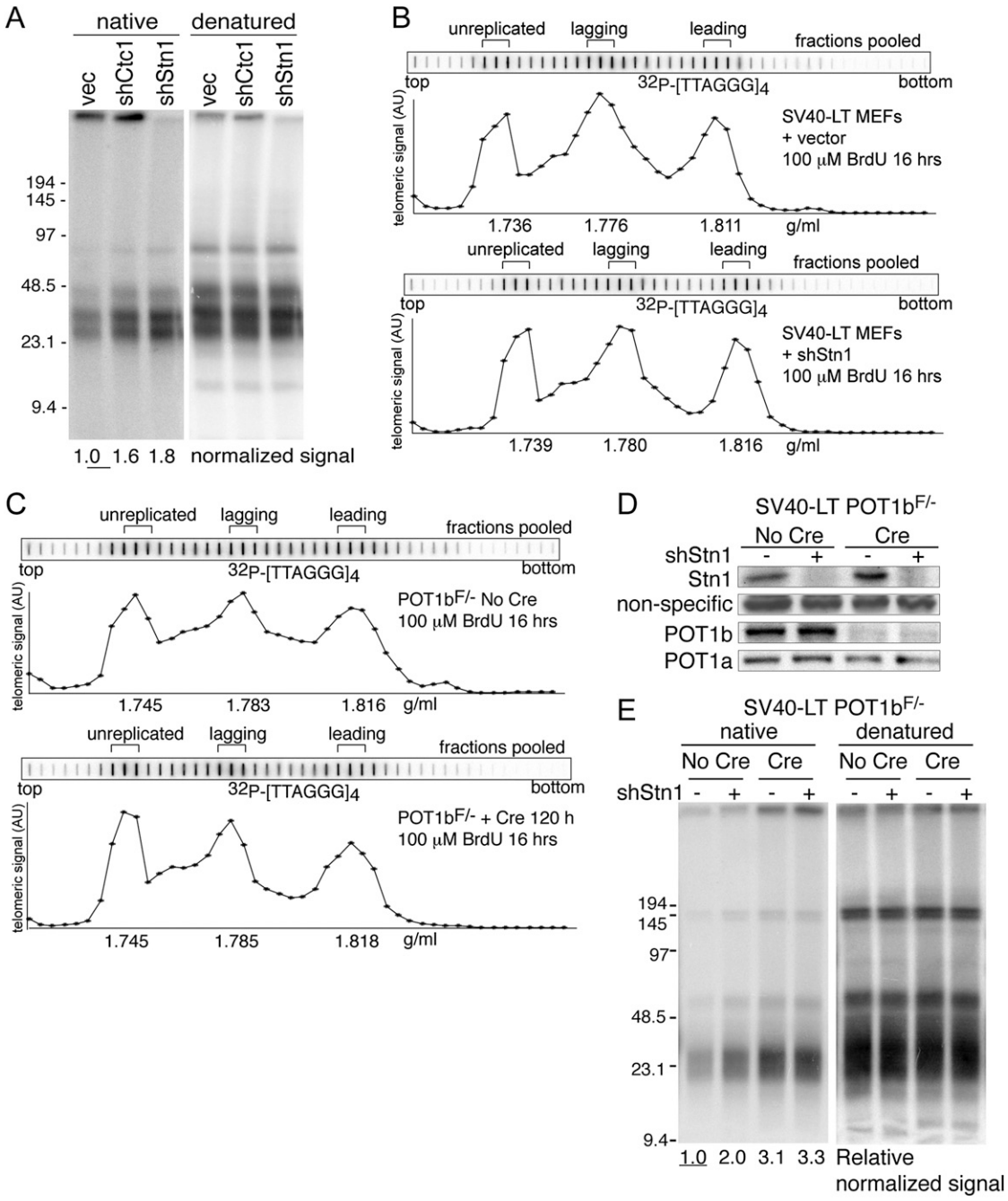

Figure S4. Stn1 Limits the Overhang at Both Newly Synthesized Telomeres and Depends on POT1b, Related to Figures 3 and 4

(A) In gel overhang analysis of wild-type MEFs following shRNA depletion of Ctc1 and Stn1.

(B) Representative slot blot of telomeric signal in each fraction collected from CsCl density gradient equilibrium centrifugation of BrdU-labeled telomeric DNA from wild-type MEFs at 96 hr following lentiviral transduction of vector (top) or shRNA targeting Stn1 (bottom).

(C) Representative slot blot of telomeric signal in each fraction collected from CsCl density gradient equilibrium centrifugation of telomeric DNA from POT1b$^{F/-}$ MEFs without Cre (top) and 120 hr after Cre (bottom) labeled with BrdU for one round of replication. The fractions pooled for overhang analyses are shown.

(D) Immunoblot detection of Stn1 and POT1b in SV40LT-immortalized POT1b$^{F/-}$ MEFs at 96 hr following lentiviral shRNA to Stn1 and 120 hr after Cre. Stn1 was detected by the anti-mStn1 antibody, mPOT1b was detected by Ab 1223, and mPOT1a was detected by Ab 1221. A nonspecific band is shown as a loading control.

(E) Representative in gel overhang analysis of POT1b$^{F/-}$ cells at 96 hr following lentiviral shRNA to Stn1 and 120 hr after Cre.

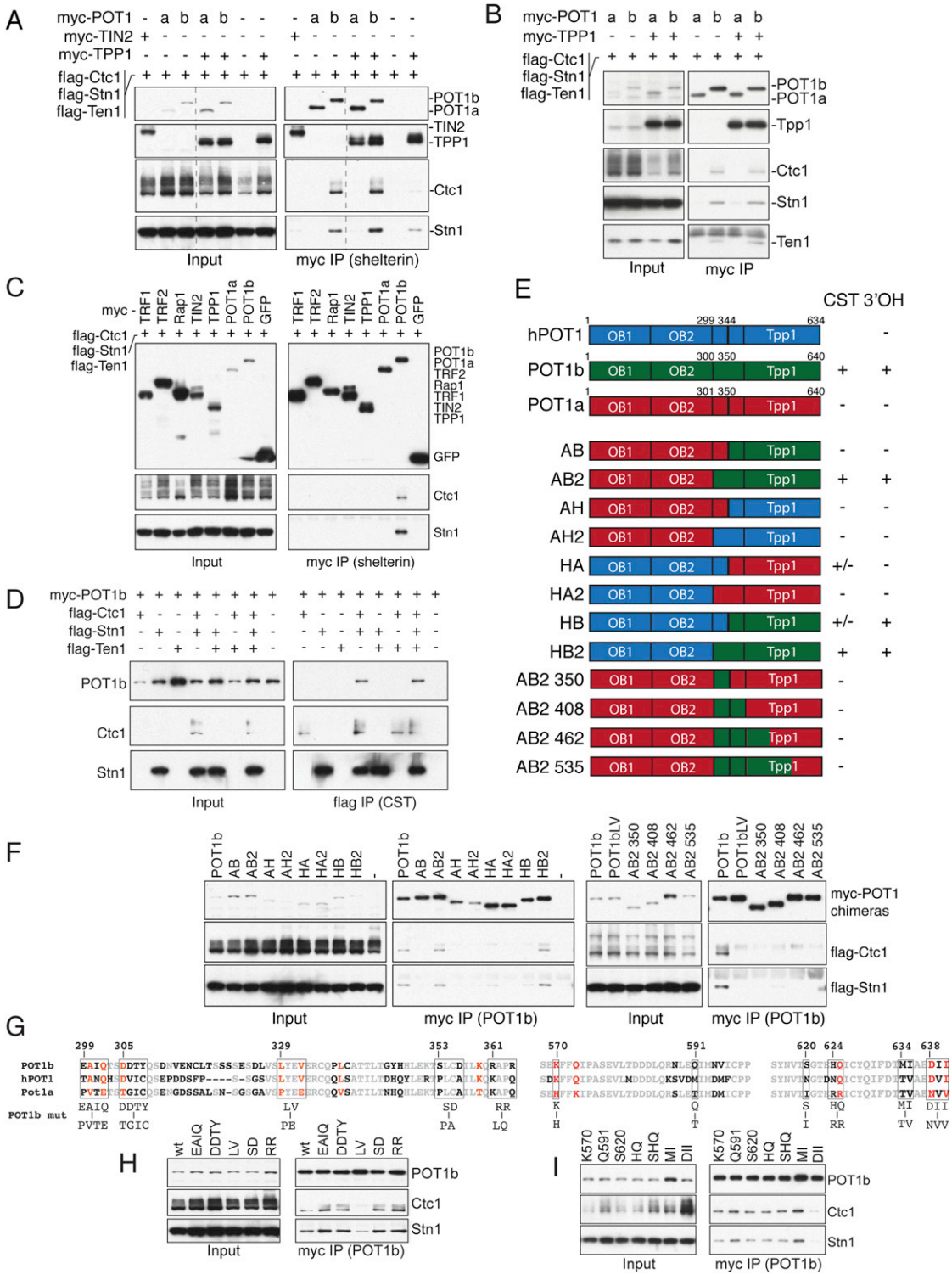

Figure S5. Characterization of the POT1b-CST Interaction, Related to Figure 5

(A) co-IP of POT1b and the Ctc1/Stn1/Ten1 (CST) complex. 293T cells were transiently cotransfected with myc-tagged POT1a or POT1b, and FLAG-tagged mCtc1, mStn1, and mTen1, in the absence or presence of myc-mTPP1. Co-IPs were performed with myc antibody. Input (left) and IPs (right) were analyzed by immunoblotting for myc (top) and FLAG (bottom).

(B) Co-IP of POT1b and the CST complex, showing the presence of Ten1 in the complex that associates with POT1b. Co-IP was performed as described in A.

(C) Co-IP of shelterin components with the CST complex. 293T cells were transiently cotransfected with individual myc-tagged shelterin components along with FLAG-tagged mCtc1, mStn1, and mTen1. Co-IPs were performed with anti-myc antibody. Input (left) and IPs (right) were analyzed by immunoblotting for myc (top) and FLAG (middle, bottom).
(D) Co-IP of POT1b with individual CST components. 293T cells were cotransfected with myc-tagged POT1b and FLAG-tagged mCtc1, mStn1, and/or mTen1 as indicated. Co-IPs were performed with the anti-FLAG antibody. Input (left) and IPs (right) were analyzed by immunoblotting for myc (top) and FLAG (middle, bottom).
(E) Schematic drawings of the domain organization of POT1 proteins and POT1 chimeras (left). The ability of the indicated POT1 chimeras to interact with the CST complex and to prevent the inappropriate resection of the telomeric 5′ end (3′OH) in POT1b-depleted MEFs (Palm and de Lange, 2008) are summarized (right). POT1a (red), POT1b (green), and hPOT1 (blue) were divided into N- and C-terminal portions between the second OB fold (OB2) of the DNA binding domain and the TPP1 interaction domain and fused in various combinations shown (see Material and Methods for the detail).
(F) Co-IPs of POT1 chimeras/mutants with the CST complex. 293T cells were transiently cotransfected with the indicated myc-tagged POT1 mutant and FLAG-tagged Ctc1, Stn1 and Ten1. Co-IPs were performed with the myc antibody. Inputs and IPs were analyzed by immunoblotting for myc (top) and FLAG (middle, bottom).
(G) Sequence alignment of regions in the C-terminal domain of human POT1, mouse POT1a, and mouse POT1b. Residues conserved among all three POT1 proteins are shown in gray. Residues conserved between hPOT1 and POT1b but not POT1a are shown in red. Residues that were changed to generate POT1b mutants are indicated with boxes.
(H) and (I) Co-IPs of the indicated myc-POT1b mutants with FLAG-tagged CST. Inputs and IPs (myc) were analyzed by immunoblotting for myc (top) and FLAG (middle, bottom).

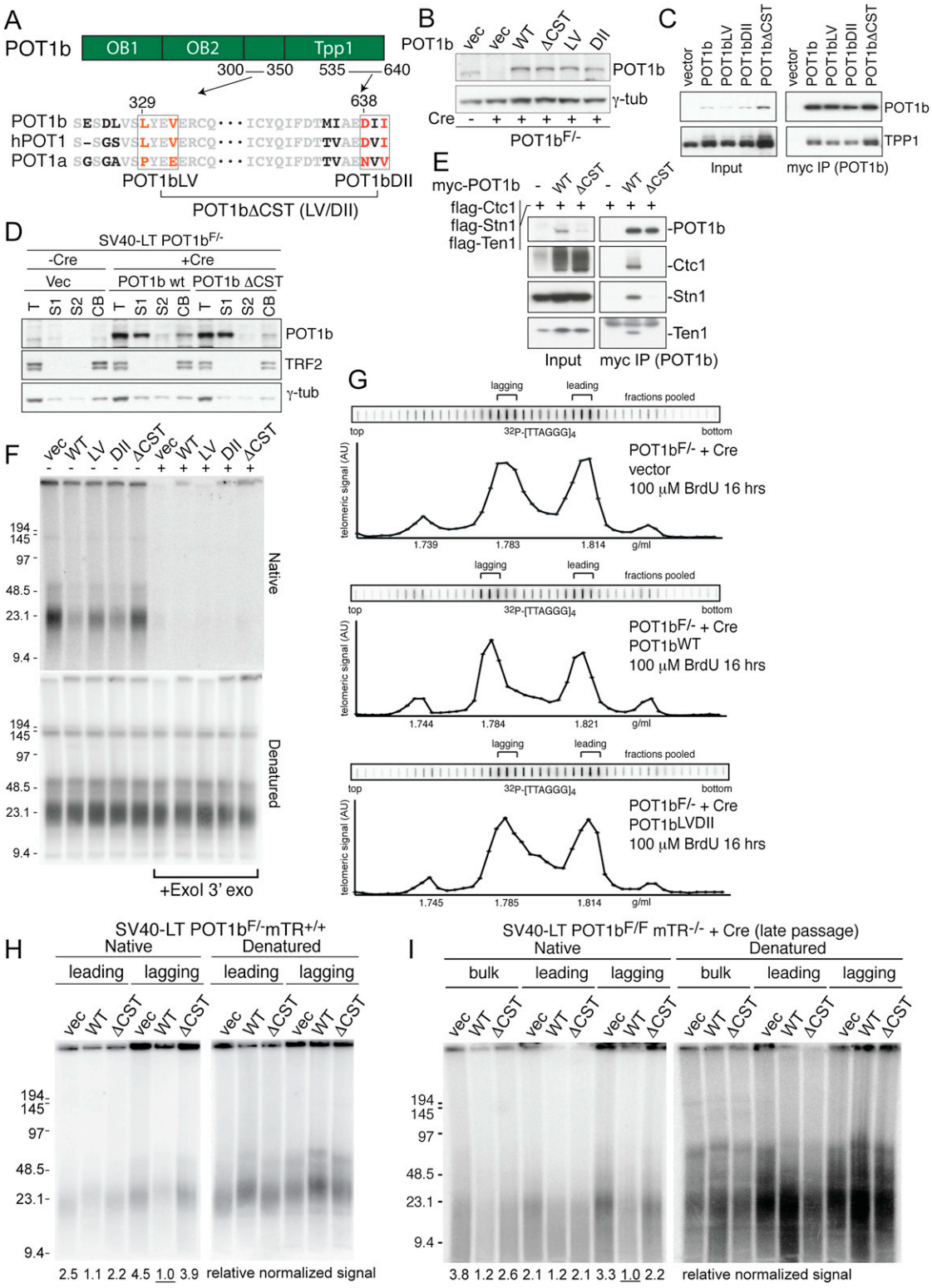

Figure S6. A POT1b Mutant Unable to Interact with CST, Related to Figure 5

(A) Schematic drawing of the POT1bΔCST mutant. The altered residues are outlined with boxes.

(B) Immunoblot detection of POT1b mutants expressed in POT1b$^{F/-}$ MEFs after Cre-mediated deletion of endogenous POT1b.

(C) Co-IP of POT1b mutants with TPP1. 293T cells were transiently transfected with the indicated myc-tagged POT1b alleles and FLAG-tagged TPP1. IPs were performed with anti-myc antibody. Input (left) and IPs (right) were analyzed by immunoblotting for myc (top) and FLAG (bottom).
(D) POT1b$^{F/-}$ cells expressing vector, wild-type POT1b, or POT1bΔCST were fractionated after infection with or without Cre. Whole-cell lysate (T), cytoplasmic proteins (S1), nucleoplasmic proteins (S2), and chromatin-bound proteins (CB) were analyzed by immunoblotting. TRF2 was used as a control for chromatin-bound proteins and γ-tubulin was used as a loading control.
(E) Co-IPs of POT1b and the CST complex. 293T cells were transiently cotransfected with myc-tagged POT1b or POT1bΔCST, and FLAG-tagged mCtc1, mStn1, and mTen1. Co-IPs were performed with the myc antibody. The CST complex associates with wild-type POT1b but not with POT1bΔCST.
(F) In gel overhang analysis of POT1b KO MEFs expressing the indicated POT1b alleles (lanes 1-6), shown next to the same samples pretreated with *E. coli* 3′ exonuclease ExoI (lanes 7-12).
(G) Representative slot blots of the telomeric signal in each fraction collected from CsCl density gradient equilibrium centrifugation of BrdU-labeled telomeric DNA from POT1b$^{F/-}$ MEFs expressing vector, wild-type POT1b, or POT1bΔCST, after the deletion of endogenous POT1b with Cre.
(H) In gel overhang analysis of separated leading- and lagging-end telomeres from POT1b$^{F/-}$ MEFs expressing vector control, wild-type POT1b, or POT1bΔCST. Endogenous POT1b was deleted by Cre-mediated gene deletion. The relative normalized overhang signal was determined with the lane containing lagging-end telomeres in cells expressing wild-type POT1b set to 1.
(I) In gel overhang analysis of separated leading- and lagging-end telomeres from POT1b$^{-/-}$mTR$^{-/-}$ MEFs (late PD) expressing vector control, wild-type POT1b, or POT1bΔCST. The relative normalized overhang signal was determined with the lane containing lagging-end telomeres in cells expressing wild-type POT1b set to 1.

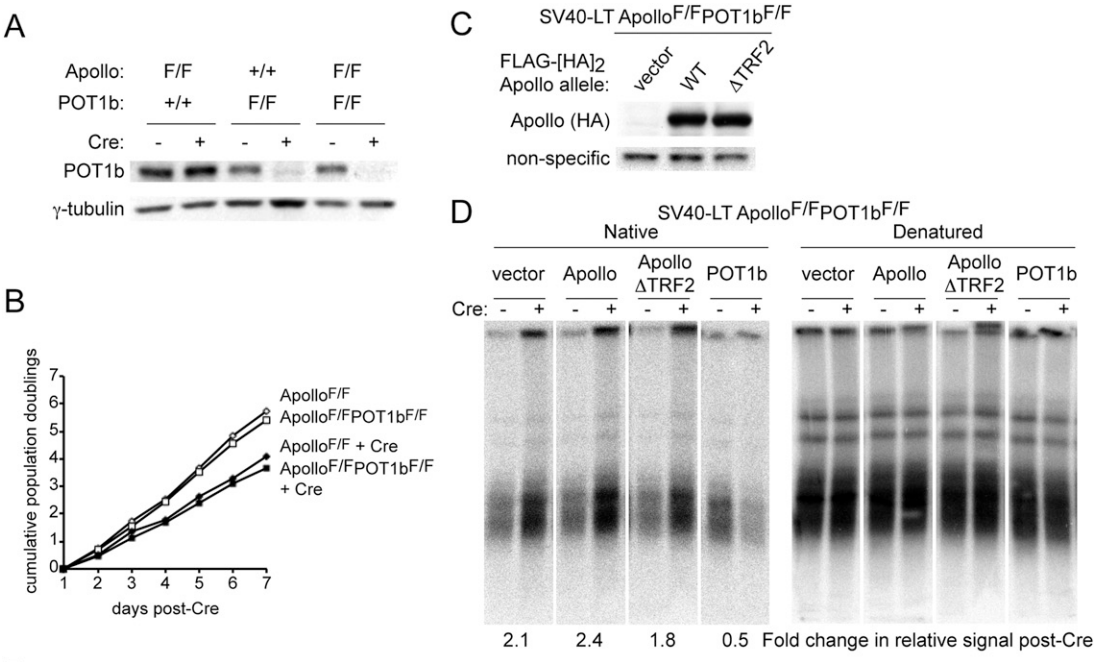

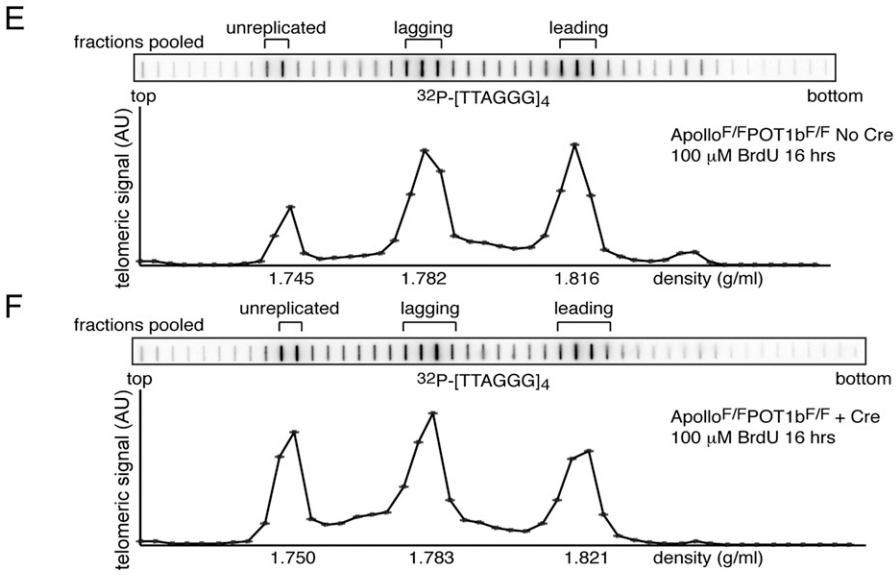

G

	% chromosomes fused leading-leading	% chromosomes fused all others
ApolloF/F + Cre (n=1086)	10.1	1.7
ApolloF/FPOT1bF/F + Cre (n=1367)	9.2	2.9

Figure S7. Accumulation of Excess Overhangs upon POT1b Deletion Partially Depends upon Apollo, Related to Figure 6

(A) Immunoblot detection of POT1b at 120 hr after Cre in SV40LT-immortalized Apollo$^{F/F}$, POT1b$^{F/F}$, and Apollo$^{F/F}$POT1b$^{F/F}$ MEFs.

(B) Growth curve of SV40LT-immortalized Apollo$^{F/F}$ and Apollo$^{F/F}$POT1b$^{F/F}$ MEFs with or without treatment with Hit&Run Cre.

(C) Immunoblot detection of FLAG-[HA]2-tagged Apollo alleles expressed in SV40LT-immortalized Apollo$^{F/F}$POT1b$^{F/F}$ MEFs. HA.11 antibody was used to detect exogenously-introduced Apollo.

(D) Representative in gel overhang analysis of SV40LT-immortalized Apollo$^{F/F}$POT1b$^{F/F}$ MEFs expressing Apollo alleles in the absence and presence of hygromycin-selectable pWzl-Cre.

(E and F) Representative slot blots of the telomeric signal in each fraction collected from CsCl density gradient equilibrium centrifugation of BrdU-labeled telomeric DNA from Apollo$^{F/F}$POT1b$^{F/F}$ MEFs in the absence of Cre (E) and at 120 hr after Hit&Run Cre (F). The fractions pooled for overhang analyses are shown.

(G) Quantification of CO-FISH analysis to detect telomere fusions in Apollo$^{F/F}$POT1b$^{F/F}$ MEFs after Cre.